Appendix A.11:

Carisbrooke Playground – VsVp 57193

Table 1: Site Description for Carisbrooke Playground (v_sv_p 57193).

Attribute	Yes/No			Description/Date	Symbol in Figure 1
	10-m Buffer	20-m Buffer	50-m Buffer		
Near a body of surface water or other free face features?	No	No	No	The center of the site is 540 meters away from the Avon River.	NA
Lateral spreading observed during the CES?	No	No	No	Ground cracks indicating lateral spreading were not observed by the mapping team.[1]	NA
Nearby buildings or structures?	No	No	Yes	Residential buildings cover 21% of the 50-m buffer.	White Fill + Brown Outline
Sloping land?	Yes	Yes	Yes	Play mounds.	NA
Step changes in the ground surface?	Yes	Yes	Yes	Play mounds.	NA
Retaining walls?	No	No	No	NA	NA
Vegetation?	Yes	Yes	Yes	Trees cover 8% of the 10-m buffer, 9% of the 20-m buffer, while trees and bushes cover 14% of the 50-m buffer. They affect all quadrants of the buffers; however, the majority is in the E half of the 50-m buffer.	White Fill + Green Outline
Anthropogenic changes to the site between the LiDAR surveys?	No	No	No	NA	NA
Other important factors?	Yes	Yes	Yes	Road covers 16% of the 20-m buffer and 14% of the 50-m buffer. Motor vehicles are occasionally parked on the road. The basketball court occupies 16% of the 10-m buffer and 7% of the 20-m buffer. The playground contains equipment in the W half of the buffers and is outlined by short wooden poles (and chain) in the NE, SE, and SW quadrants.	Road: White Fill + Gray Outline; Poles: White Fill + Orange Outline; Equipment: White Fill + Purple Outline

Note: Buffer is the area within a circle of a specified radius with VsVp investigations done at its center (172.709944°, -43.510815°).

[1] Canterbury Geotechnical Database. (2012). "Observed Ground Crack Locations", Map Layer CGD0400 - 23 July 2012, retrieved July 09, 2018 from https://canterburygeotechnicaldatabase.projectorbit.com/

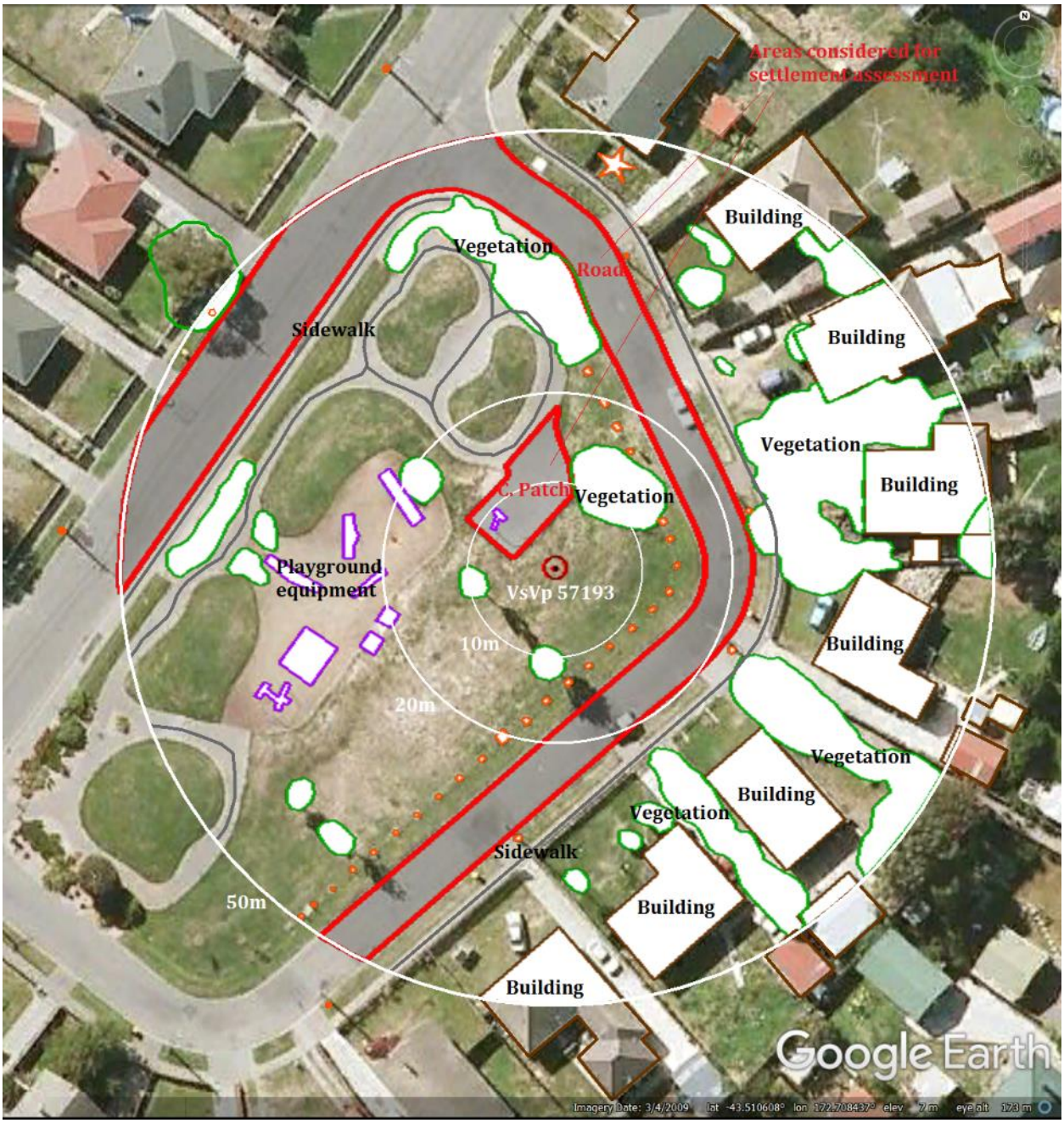

Figure 1: Site plan with areas where LiDAR survey data is considered.

Note 1: The selected patch in the free field is level, free of vegetation, and structures, all of which have the potential to influence LiDAR surveys. The entire portion of the road within the 50-m buffer was considered for settlement assessment.

Table 2: LiDAR flight error adjustments, global adjustments for the difference between average LiDAR point elevations and benchmark survey elevations, and vertical tectonic movement adjustments.

	Adjustments (mm)		
Earthquake Event(s)	LiDAR Flight Error	Global Offset[2]	Tectonic Vertical Movement
Sep-10	0	-3	0
Feb-11	0	16	-25
Jun-11	0	38	-50
Dec-11	0	-65	10
CES	0	-14	-65
Any LiDAR survey affected by ejecta?*			"Yes"

Note: The negative sign indicates the subtraction from the ground surface subsidence, while the positive sign indicates the addition to the ground surface subsidence; * indicates that the Sep-10 LiDAR survey overestimated the ground surface elevation of Paved Patch due to the presence of sediments before any earthquake event occurred so 10 mm of ground surface subsidence is added for the Sep-10 EQ and subtracted for the Feb-11 EQ.

Table 3a: LiDAR Measurement Error for Concrete Patch.

Surveys	Buffer	Area Averaged Difference Indicating Repeat Measurement Error (mm)	$\sigma^*_{individual\ LiDAR\ points}$ (mm)	%Reduction in σ due to Area Averaging of LiDAR Points
Post Feb 2011: Mar 2011 and May 2011	10-m	ND	59	[93,93]
	20-m	55		
	50-m	55		
Post Dec 2011: Feb 2012 and Oct 2015	10-m	ND	70	[6,6]
	20-m	4		
	50-m	4		

*Standard deviation; ND = Not determined.

[2] Russell, J., & van Ballegooy, S. (2015). *Canterbury Earthquake Sequence: Increased liquefaction vulnerability assessment methodology*. New Zealand: Tonkin & Taylor Ltd.

Table 3b: LiDAR Measurement Error for Road.

Surveys	Buffer	Area Averaged Difference Indicating Repeat Measurement Error (mm)	$\sigma^*_{individual\ LiDAR\ points}$ (mm)	%Reduction in σ due to Area Averaging of LiDAR Points
Post Feb 2011: Mar 2011 and May 2011	10-m	NA	59	[131,134]
	20-m	77		
	50-m	79		
Post Dec 2011: Feb 2012 and Oct 2015	10-m	NA	70	[7,39]
	20-m	5		
	50-m	27		

*Standard deviation; NA= Not available.

Table 4a: Ground surface subsidence adjustments due to LiDAR measurement error for Concrete Patch.

Earthquake Event(s)	$\sigma_{pre\text{-}EQ\ LiDAR\ survey}$ (mm)	$\sigma_{post\text{-}EQ\ LiDAR\ survey}$ (mm)	σ_{total} (mm)	Area Average Adjusted σ (mm) **
Sep-10	158	56	134	±125
Feb-11	56	59	59	±55
Jun-11	59	61	62	±58
Dec-11	61	70	87	±81
CES	158	70	124	±116

**Based on the highest %Reduction in Table 3.

Table 4b: Ground surface subsidence adjustments due to LiDAR measurement error for Road.

Earthquake Event(s)	$\sigma_{pre\text{-}EQ\ LiDAR\ survey}$ (mm)	$\sigma_{post\text{-}EQ\ LiDAR\ survey}$ (mm)	σ_{total} (mm)	Area Average Adjusted σ (mm) **
Sep-10	158	56	134	±180
Feb-11	56	59	59	±79
Jun-11	59	61	62	±83
Dec-11	61	70	87	±116
CES	158	70	124	±167

**Based on the highest %Reduction in Table 3.

Table 5a: Raw liquefaction-related ground surface subsidence using original LiDAR points for Concrete Patch.

	Average Ground Surface Subsidence (mm)		
Earthquake Event(s)	10-m Buffer	20-m Buffer	50-m Buffer
Sep-10	31	31	31
Feb-11	121	121	121
Jun-11	80	80	80
Dec-11	13	13	13
CES	245	245	245

Table 5b: Raw liquefaction-related ground surface subsidence using original LiDAR points for Road.

	Average Ground Surface Subsidence (mm)		
Earthquake Event(s)	10-m Buffer	20-m Buffer	50-m Buffer
Sep-10	NA	79	-6
Feb-11	NA	113	137
Jun-11	NA	89	127
Dec-11	NA	14	-38
CES	NA	295	220

Table 6a: Corrected liquefaction-related ground surface subsidence for Concrete Patch using original LiDAR points with the calculated adjustments in Table 2.

	Average Calculated Ground Surface Subsidence (mm)		
Earthquake Event(s)	10-m Buffer	20-m Buffer	50-m Buffer
Sep-10	ND	38±125	38±125
Feb-11	ND	102±50	102±50
Jun-11	ND	68±50	68±50
Dec-11	ND	-42±75	-42±75
CES	ND	166±125	166±125

Notes: Plus/minus values are same as those in Table 4, but rounded to the nearest 25; Positive overall values indicate ground surface subsidence, while negative overall values indicate ground surface uplift.

Table 6b: Corrected liquefaction-related ground surface subsidence for Road using original LiDAR points with the calculated adjustments in Table 2.

	Average Calculated Ground Surface Subsidence (mm)		
Earthquake Event(s)	10-m Buffer	20-m Buffer	50-m Buffer
Sep-10	NA	76±175	-9±175
Feb-11	NA	104±75	128±75
Jun-11	NA	77±75	115±75
Dec-11	NA	-41±125	-93±125
CES	NA	216±175	141±175

Notes: Plus/minus values are same as those in Table 4, but rounded to the nearest 25; Positive overall values indicate ground surface subsidence, while negative overall values indicate ground surface uplift.

Table 7a: Corrected liquefaction-related ground surface subsidence for Concrete Patch using LiDAR DEMs.

	Estimated Ground Surface Subsidence (mm)								
	10-m Buffer			20-m Buffer			50-m Buffer		
Earthquake Event(s)	16th %ile	50th %ile	84th %ile	16th %ile	50th %ile	84th %ile	16th %ile	50th %ile	84th %ile
Sep-10	50	50	50	50	50	50	50	50	50
Feb-11	100	150	150	100	150	150	100	150	150
Jun-11	50	50	50	50	50	50	50	50	50
Dec-11	50	50	50	50	50	50	50	50	50
CES	250	250	250	150	250	250	150	250	250

Note: These percentiles are not the exact statistical measures; they indicate the spatial variability of ground surface subsidence.

Table 7b: Corrected liquefaction-related ground surface subsidence for Road using LiDAR DEMs.

	Estimated Ground Surface Subsidence (mm)								
	10-m Buffer			20-m Buffer			50-m Buffer		
Earthquake Event(s)	16th %ile	50th %ile	84th %ile	16th %ile	50th %ile	84th %ile	16th %ile	50th %ile	84th %ile
Sep-10	NA	NA	NA	50	50	150	50	50	150
Feb-11	NA	NA	NA	100	150	150	50	150	150
Jun-11	NA	NA	NA	50	50	50	50	50	50
Dec-11	NA	NA	NA	50	50	50	50	50	50
CES	NA	NA	NA	250	250	250	150	250	350

Note: These percentiles are not the exact statistical measures; they indicate the spatial variability of ground surface subsidence.

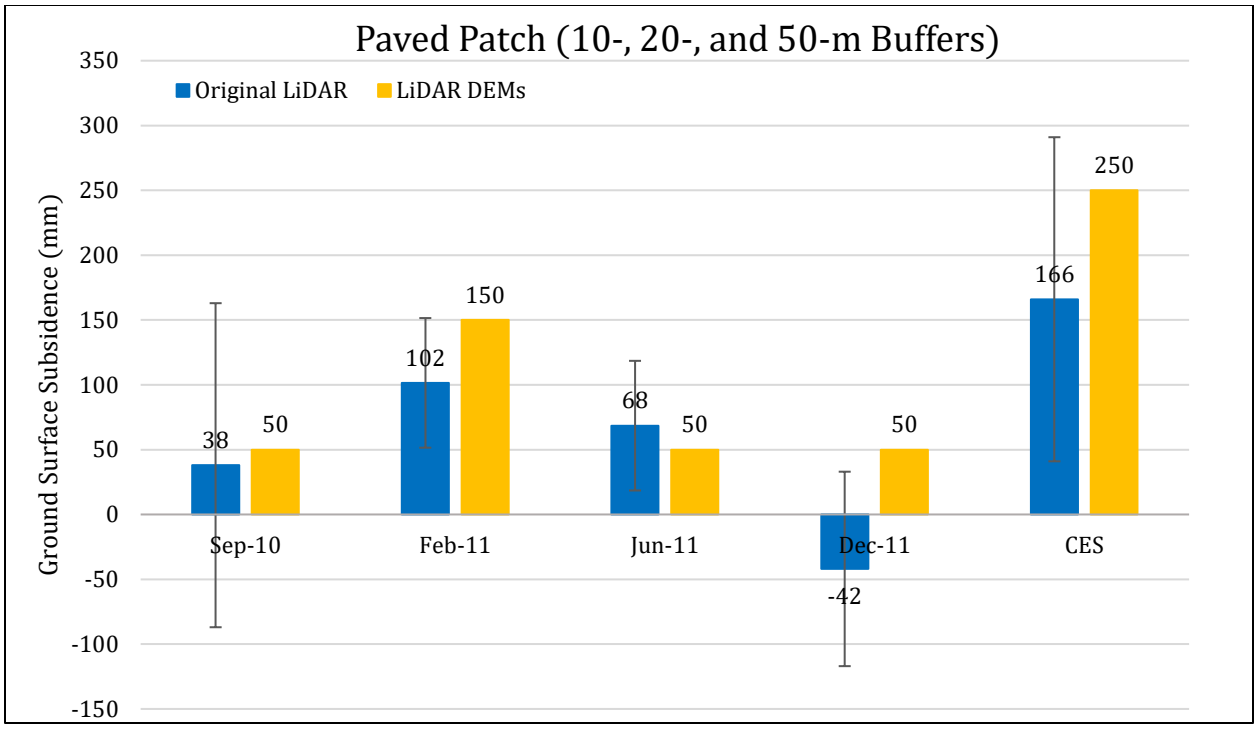

Figure 2: Comparison between ground surface subsidence determined from original LiDAR survey points and ground surface subsidence (50th %ile) estimated using LiDAR DEMs for Concrete Patch within the 10-m buffer.

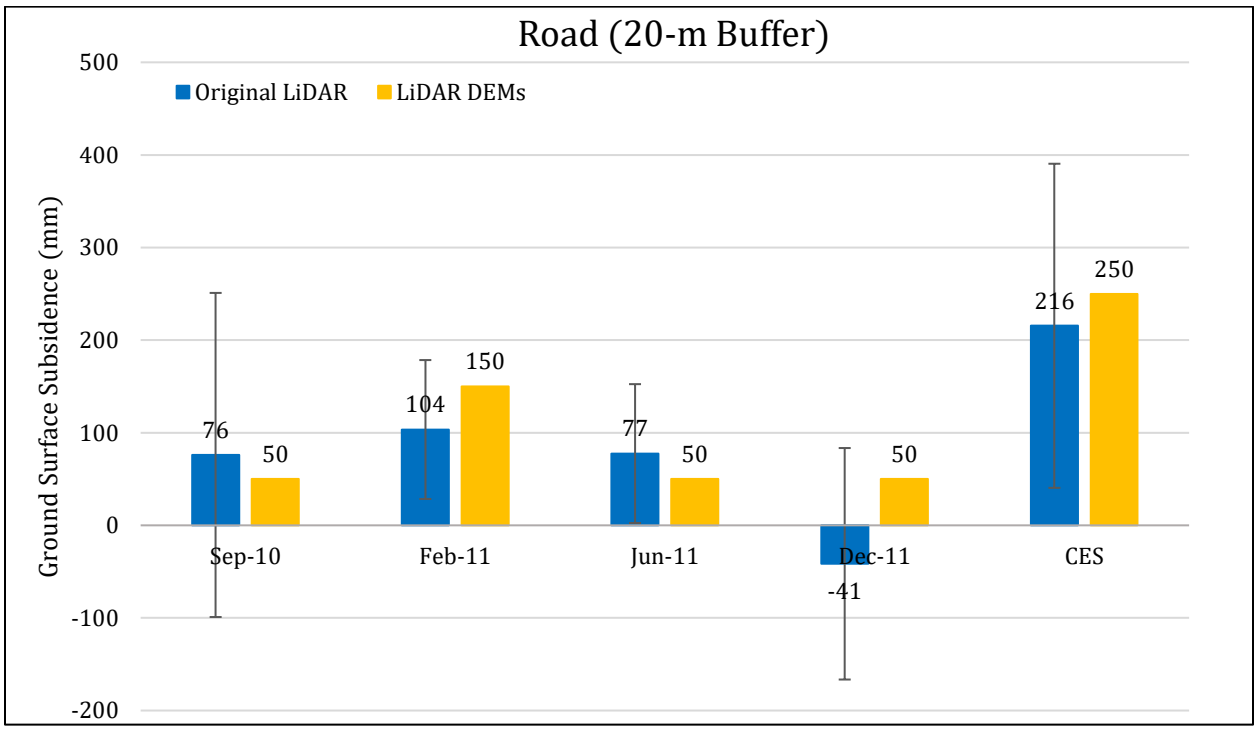

Figure 3: Comparison between ground surface subsidence determined from original LiDAR survey points and ground surface subsidence (50th %ile) estimated using LiDAR DEMs for Road within the 20-m buffer.

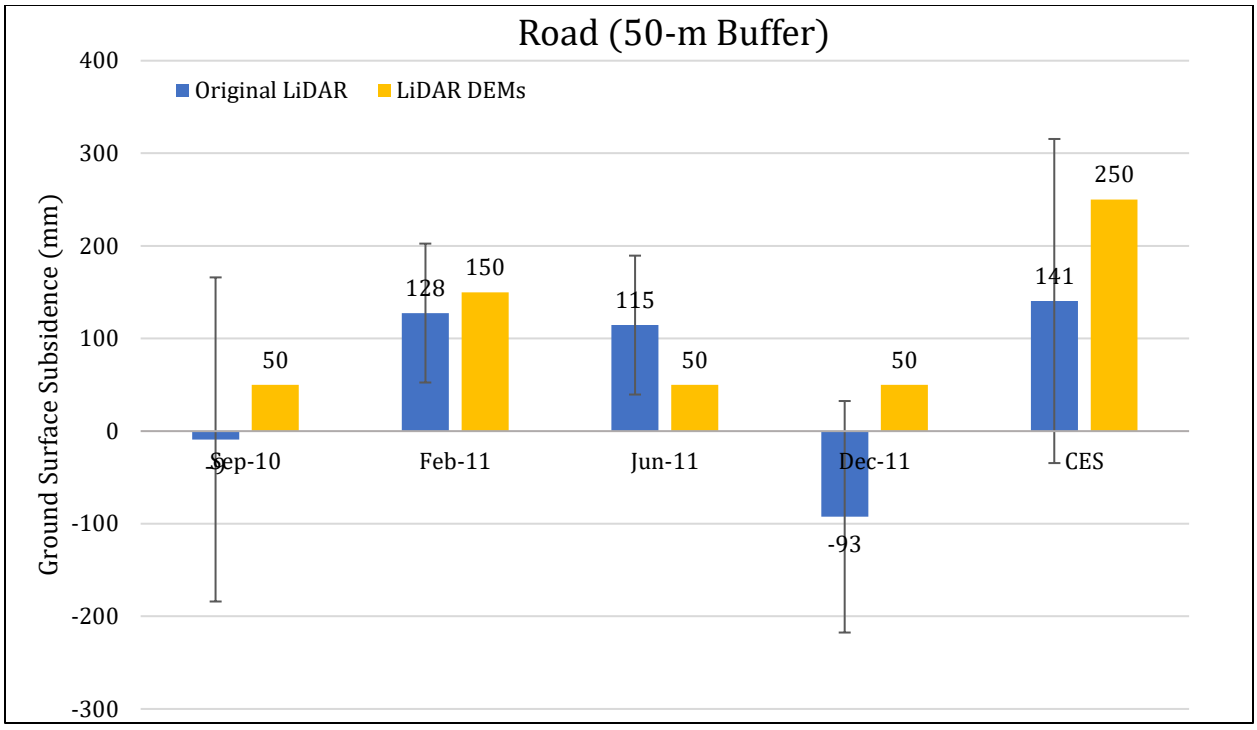

Figure 4: Comparison between ground surface subsidence determined from original LiDAR survey points and ground surface subsidence (50th %ile) estimated using LiDAR DEMs for Road within the 20-m buffer.

Note 2: The ground surface subsidence values determined from original LiDAR survey points are generally similar to the ground surface subsidence values estimated using LiDAR DEMs for all earthquake events.

Table 8a: Ejecta-induced settlement for the top 20-m of the soil profile for Concrete Patch within the 20-m and 50-m buffers for the 50th %ile PGA and P_L=50% using BI-2014, ZRB-2002, C_{FC} = 0.13, and I_C cutoff of 2.6.

Earthquake Event(s)	M_W	PGA (g)	Depth to Groundwater (m)	S_T (mm)	S_{V1D} (mm)	$S_{E,L}$ (mm)
Sep-10	7.1	0.18	2.8	38±125	1±20	37±127
Feb-11	6.2	0.47	2.8	102±50	41±50	61±71
Jun-11	6.2	0.28	3.3	68±50	3±25	65±56
Dec-11	6.1	0.35	2.5	-42±75	7±50	-49±90

Notes: S_T = Total settlement (Table 6); S_{V1D} = Average vertical settlement due to volumetric compression using Boulanger and Idriss (2014) (BI-2014), Zhang et al. (2002) (ZRB-2002) procedures and de Greef and Lengkeek (2018) thin-layer correction; $S_{E,L}$ = Ejecta-induced settlement as the difference between the LiDAR-based S_T and S_{V1D}.

Table 8b: Ejecta-induced settlement for the top 20-m of the soil profile for Road within the 20-m buffer for the 50th %ile PGA and P_L=50% using BI-2014, ZRB-2002, C_{FC} = 0.13, and I_c cutoff of 2.6.

Earthquake Event(s)	M_W	PGA (g)	Depth to Groundwater (m)	S_T (mm)	S_{V1D} (mm)	$S_{E,L}$ (mm)
Sep-10	7.1	0.18	2.8	76±175	1±20	75±176
Feb-11	6.2	0.47	2.8	104±75	60±50	44±90
Jun-11	6.2	0.28	3.3	77±75	6±25	71±79
Dec-11	6.1	0.35	2.5	-41±125	7±50	-48±135

Notes: S_T = Total settlement (Table 6); S_{V1D} = Average vertical settlement due to volumetric compression using Boulanger and Idriss (2014) (BI-2014), Zhang et al. (2002) (ZRB-2002) procedures and de Greef and Lengkeek (2018) thin-layer correction; $S_{E,L}$ = Ejecta-induced settlement as the difference between the LiDAR-based S_T and S_{V1D}.

Table 8c: Ejecta-induced settlement for the top 20-m of the soil profile for Road within the 50-m buffer for the 50th %ile PGA and P_L=50% using BI-2014, ZRB-2002, C_{FC} = 0.13, and I_c cutoff of 2.6.

Earthquake Event(s)	M_W	PGA (g)	Depth to Groundwater (m)	S_T (mm)	S_{V1D} (mm)	$S_{E,L}$ (mm)
Sep-10	7.1	0.18	2.8	-9±175	1±20	-10±176
Feb-11	6.2	0.47	2.8	128±75	60±50	68±90
Jun-11	6.2	0.28	3.3	115±75	6±25	109±79
Dec-11	6.1	0.35	2.5	-93±125	7±50	-100±135

Notes: S_T = Total settlement (Table 6); S_{V1D} = Average vertical settlement due to volumetric compression using Boulanger and Idriss (2014) (BI-2014), Zhang et al. (2002) (ZRB-2002) procedures and de Greef and Lengkeek (2018) thin-layer correction; $S_{E,L}$ = Ejecta-induced settlement as the difference between the LiDAR-based S_T and S_{V1D}.

Note 3: The uncertainty for volumetric settlement was derived based on the sensitivity of volumetric settlement to PGA, C_{FC}, and P_L for each earthquake event for VsVp 57203 *Shirley Intermediate School* and CC LIQ 1 – CPT 5586 – *Vivian St* sites. Taking the 50th percentile as the baseline case, the minimum and maximum values corresponding to the difference between the 25th percentile and the 50th percentile and the 75th percentile and the 50th percentile were determined. The arithmetic mean of the range of the minimum and maximum difference was evaluated for each patch at the two sites. The maximum arithmetic mean for each earthquake event was rounded to the nearest five and used as the uncertainty value. Accordingly, the 1-D volumetric settlement uncertainties of ±20, ±50, ±25, and ±50 mm for the Sep-10, Feb-11, Jun-11, and Dec-11 earthquake events, respectively, were used for all sites in this study.

Table 9a: Coverage area and height of ejecta estimates for Concrete Patch within the 20-m and 50-m buffers using photographs.

Earthquake Event	$A_{E,thick}$ (m^2)	$H_{E,thick}$ (mm)	$A_{E,thin}$ (m^2)	$H_{E,thin}$ (m)	A_T (m^2)
Sep-10	0	0	0	0	96.9
Feb-11	0	0	37.9	3-6	96.9
Jun-11	0	0	0	0	96.9
Dec-11	0	0	0	0	96.9

Notes: $A_{E,thick/thin}$ =Coverage area of thick/thin ejecta layers; $H_{E,thick/thin}$ = Lower-upper estimate of height of thick/thin ejecta layers; A_T = Total assessment area of a buffer being considered; Thin and thick layers correspond to light gray and dark gray colors of ejecta observed in aerial photographs.

Table 9b: Coverage area and height of ejecta estimates for Road within the 20-m buffer using photographs.

EQ Event	$H_{E,thin}$ (mm)	$A_{E,thin}$ (m^2)	$H_{E,thick}$ (mm)	$A_{E,thick}$ (m^2)	A_T (m^2)
Sep-10	0	0	0	0	182
Feb-11	3-6	49.4	0	0	187
Jun-11	0	0	0	0	182
Dec-11	0	0	0	0	182

Notes: $A_{E,thin/thick}$ = Coverage area of thin/thick ejecta layers; $H_{E,\ thin/thick}$ = Lower-upper estimate of height of thin/thick ejecta layers; A_T= Total assessment area of a buffer being considered; Thin and thick layers correspond to light gray and dark gray colors of ejecta observed in aerial photographs.

Table 9b: Coverage area and height of ejecta estimates for Road within the 50-m buffer using photographs.

EQ Event	$H_{E,thin}$ (mm)	$A_{E,thin}$ (m^2)	$H_{E,thick}$ (mm)	$A_{E,thick}$ (m^2)	$H_{E,prism/pyr}$ (mm)	$V_{E,prism/pyr}$ (m^3)	A_T (m^2)
Sep-10	0	0	0	0	0	0	1096
Feb-11	3-6	638	15-30	7.6	5-210	3.83-6.01	1191
Jun-11	0	0	0	0	0	0	1096
Dec-11	0	0	0	0	0	0	1096

Notes: $A_{E,thin/thick}$ = Coverage area of thin/thick ejecta layers; $H_{E,\ thin/thick}$ = Lower-upper estimate of height of thin/thick ejecta layers; $H_{E,prism/pyr}$ = Lower-upper estimate of ejecta height near the curb based on 2-4% cross slope of normal crown; $V_{E,prism}$ = Lower-upper estimate of total volume of prismatic-shape ejecta; $V_{E,pyr}$ = Lower-upper estimate of total volume of pyramidal-shape ejecta; A_T= Total assessment area of a buffer being considered; Thin and thick layers correspond to light gray and dark gray colors of ejecta observed in aerial photographs.

Note 4: The values in Table 9 correspond to the coverage area of ejecta outlined in aerial photographs (Figures 64 through 67) and the lower and upper estimates of ejecta height based on geometry and ground photographs (Figure 68). Figure 62 shows the presence of sediments within Paved Patch prior to the earthquake events (Oct 2009), while the water pooled on Paved Patch is likely a result of rain showers from 3 Sep 2010 (Figure 63). The ejecta-induced settlement using the photographs and engineering judgment, $S_{E,P}$, is estimated as

$$S_{E,P} = \frac{\sum_{i=1}^{a} A_{E,thick,i} * H_{E,thick,i} + \sum_{j=1}^{b} A_{E,thin,j} * H_{E,thin,j}}{A_T} + \frac{\frac{1}{2}\sum_{n=1}^{f} W_{E,prism,n} * H_{E,prism,n} * L_{E,prism,n} + \frac{1}{3}\sum_{p=1}^{g} W_{E,pyramid,p} * H_{E,pyramid} * L_{E,pyramid}}{A_T} = \frac{\sum_{i=1}^{a} V_{E,thick,i} + \sum_{j=1}^{b} V_{E,thin,j} + \sum_{n=1}^{f} V_{E,prism,n} + \sum_{p=1}^{g} V_{E,pyramid,p}}{A_T}$$

where

- $A_{E,thick,i}$ and $H_{E,thick,i}$ are the area and the height of a thick ejecta layer, respectively;
- $A_{E,thin,j}$ and $H_{E,thin,j}$ are the area and the height of a thin ejecta layer, respectively;
- $W_{E,prism,n}$ and $L_{E,prism,n}$ are the width and the length of the coverage area of an ejecta layer shaped as a right triangular prism, respectively, and $H_{E,prism,n}$ is the height of a right triangular prism-like ejecta layer;
- $W_{E,pyr,p}$ and $L_{E,pyr,p}$ are the width and the length of the coverage area of a pyramid-like ejecta layer, respectively, and $H_{E,pyr,p}$ is the height of a pyramid-like ejecta layer;
- A_T is the total assessment area for a buffer being considered (Figure 1).

Table 10: Ejecta-induced settlement estimates for Concrete Patch and Road based on photographs.

Earthquake Event	Concrete Patch (20-m and 50-m buffers)		Road (20-m buffer)		Road (50-m buffer)	
	$S_{E,P,lower}$ (mm)	$S_{E,P,upper}$ (mm)	$S_{E,P,lower}$ (mm)	$S_{E,P,upper}$ (mm)	$S_{E,P,lower}$ (mm)	$S_{E,P,upper}$ (mm)
Sep-10	0	0	0	0	0	0
Feb-11	1	2	1	2	5	9
Jun-11	0	0	0	0	0	0
Dec-11	0	0	0	0	0	0

Note: $S_{E,P,lower}$ and $S_{E,P,upper}$ correspond to lower and upper estimates of $S_{E,P}$, respectively.

Table 11: Best final estimates of ejecta-induced settlement for Concrete Patch and Road.

EQ Event	Concrete Patch (20-m and 50-m buffers)			Road (20-m buffer)			Road (50-m buffer)		
	$S_{E,L}$ (mm)	$S_{E,P}$ (mm)	$S_{E,final}$ (mm)	$S_{E,L}$ (mm)	$S_{E,P}$ (mm)	$S_{E,final}$ (mm)	$S_{E,L}$ (mm)	$S_{E,P}$ (mm)	$S_{E,final}$ (mm)
Sep-10	37±127	0	0	75±176	0	0	-10±176	0	0
Feb-11	61±71	1.5±0.5	<5	44±90	1.5±0.5	<5	68±90	7±2	15±10
Jun-11	65±56	0	0	71±79	0	0	109±79	0	0
Dec-11	-49±90	0	0	-48±135	0	0	-100±135	0	0

Notes: $S_{E,L}$ = Ejecta-induced settlement based on LiDAR data reported in Table 8; $S_{E,P}$ = Median ejecta-induced settlement for the range of values reported in Table 10; $S_{E,final}$ = Best final estimate of ejecta-induced settlement rounded to the nearest 5; Final plus/minus values are also rounded to the nearest 5.

Note 5:

- $S_{E,final}$ due to the Sep-10, Jun-11, and Dec-11 EQs for both Concrete Patch and Road is based solely on $S_{E,P}$ because the physical evidence does not indicate the presence of ejecta following the three events.
- For the Feb-11 EQ, $S_{E,final}$ for Concrete Patch and Road within the 20-m buffer is equal to $S_{E,P}$ because they have almost no ejecta yet the LiDAR-based results suggest significant ejecta-induced settlements. For Road within the 50-m buffer, $S_{E,final}$ is a weighted average of $S_{E,L}$ and $S_{E,P}$ with the weight coefficients of 0.1 and 0.9, respectively. The uncertainty associated with $S_{E,final}$ for Road (50-m buffer) is also a weighted average of uncertainties associated with $S_{E,L}$ and $S_{E,P}$ with the same weights of 0.1 and 0.9, respectively.
- The weights are based on the LiDAR error bands, LPI prediction error (Maurer et al. 2014[3]), presence of ejecta at the time of LiDAR surveys, density of July 20113 LiDAR survey points, and completeness of visual evidence (i.e., ground and aerial photographs and EQC LDAT property inspection reports for the site). The Carisbrooke Playground site is not in the apparent zone of higher/lower ground surface subsidence for any earthquake event (i.e., the ground surface elevation is not overestimated/underestimated by any LiDAR survey). The site is in the zone of accurate LPI prediction of liquefaction severity for the Sep-10 EQ and slight to moderate LPI overprediction of liquefaction severity for the Feb-11 EQ. The LDAT property inspection report is not available for the basketball court (i.e., Concrete Patch) and there are no ground photographs of the road.

Summary:

The best estimate of the ejecta-induced free-field ground settlement at the Carisbrooke Playground site for the SEP 2010, FEB 2011, JUN 2011, and DEC 2011 earthquake is 0 mm, <5 mm, 0 mm, and 0 mm, respectively.

[3] Maurer, B. W., Green, R. A., Cubrinovski, M., & Bradley, B. A. (2014). Evaluation of the Liquefaction Potential Index for Assessing Liquefaction Hazard in Christchurch, New Zealand. *Journal of Geotechnical and Geoenvironmental Engineering*, 140(7), 04014032-1-11. doi:10.1061/(asce)gt.1943-5606.0001117

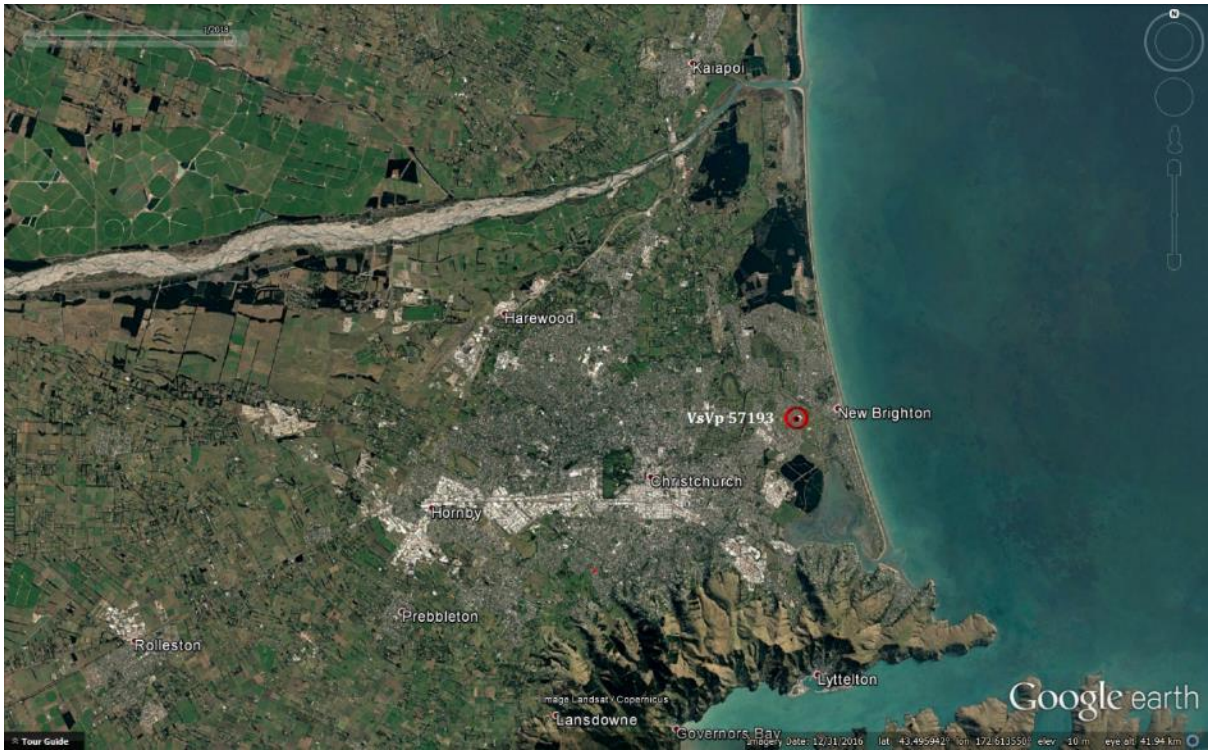

Figure 5: Location of the site.

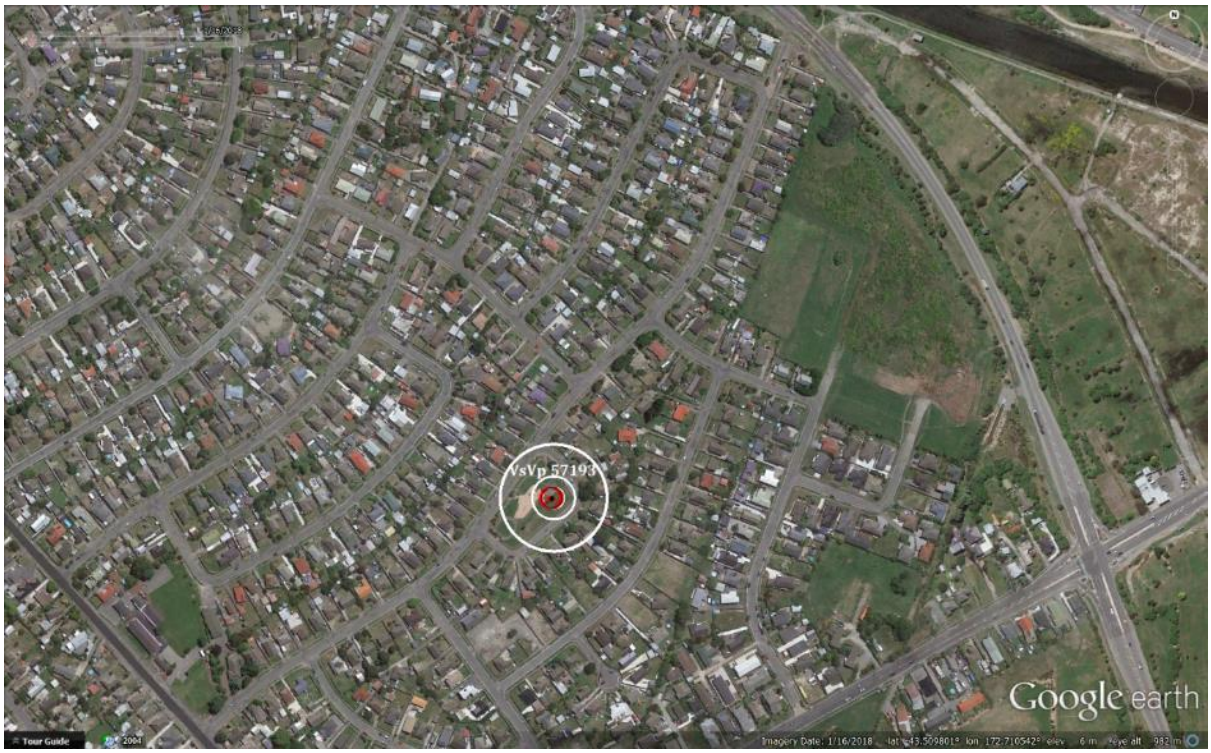

Figure 6: Position of the site relative to nearby buildings, vegetation, and free-face features.

Figure 7: Carisbrooke Sreet view of the mounds.

Figure 8: Ventnor Cres view of the mounds.

Figure 9: Satellite image of the site taken in Dec 2004.

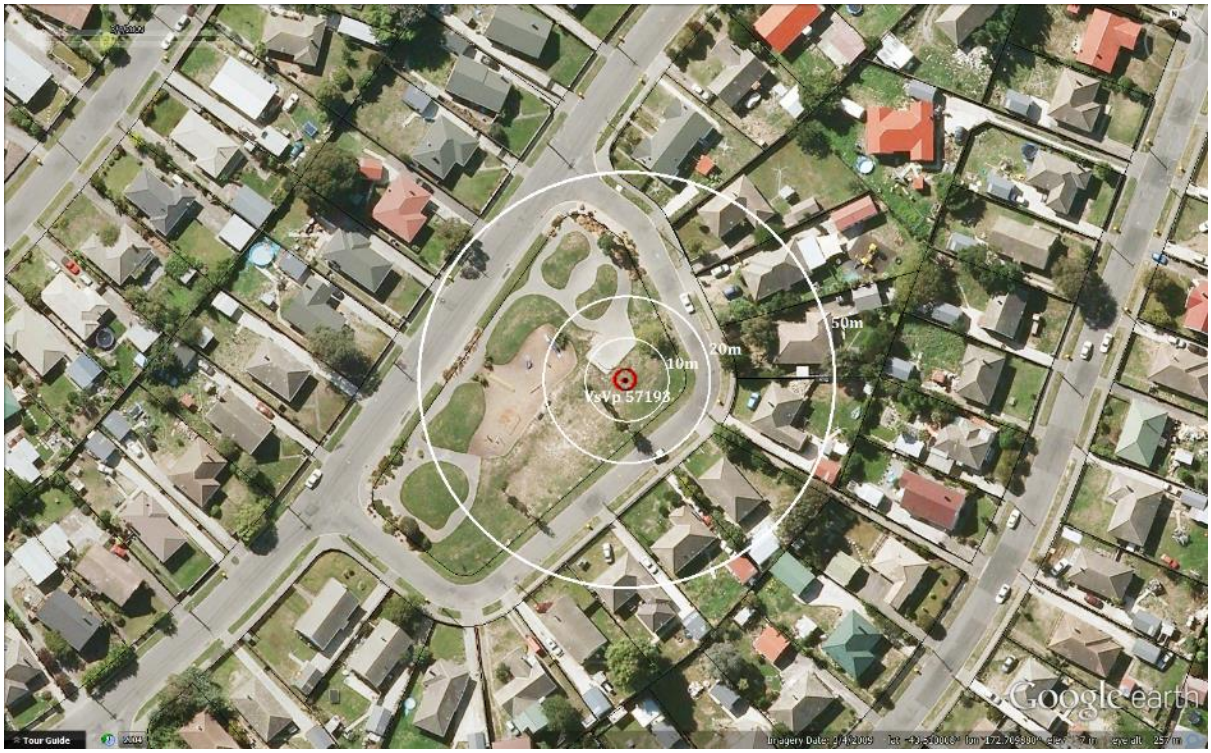

Figure 10: Satellite image of the site taken in Mar 2009.

Figure 11: Satellite image of the site taken in Sep 2010.

Figure 12: Satellite image of the site taken in Feb 2011.

Figure 13: Satellite image of the site taken in Apr 2012.

Figure 14: Satellite image of the site taken in Feb 2016.

Figure 15: EQC Aerial Photograph of the site taken Sep 4, 2010.

Figure 16: EQC Aerial Photograph of the site taken on Feb 24, 2011.

Figure 17: EQC Aerial Photograph of the site taken on June 16, 2011.

Figure 18: EQC Aerial Photograph of the site taken on Dec 24, 2012.

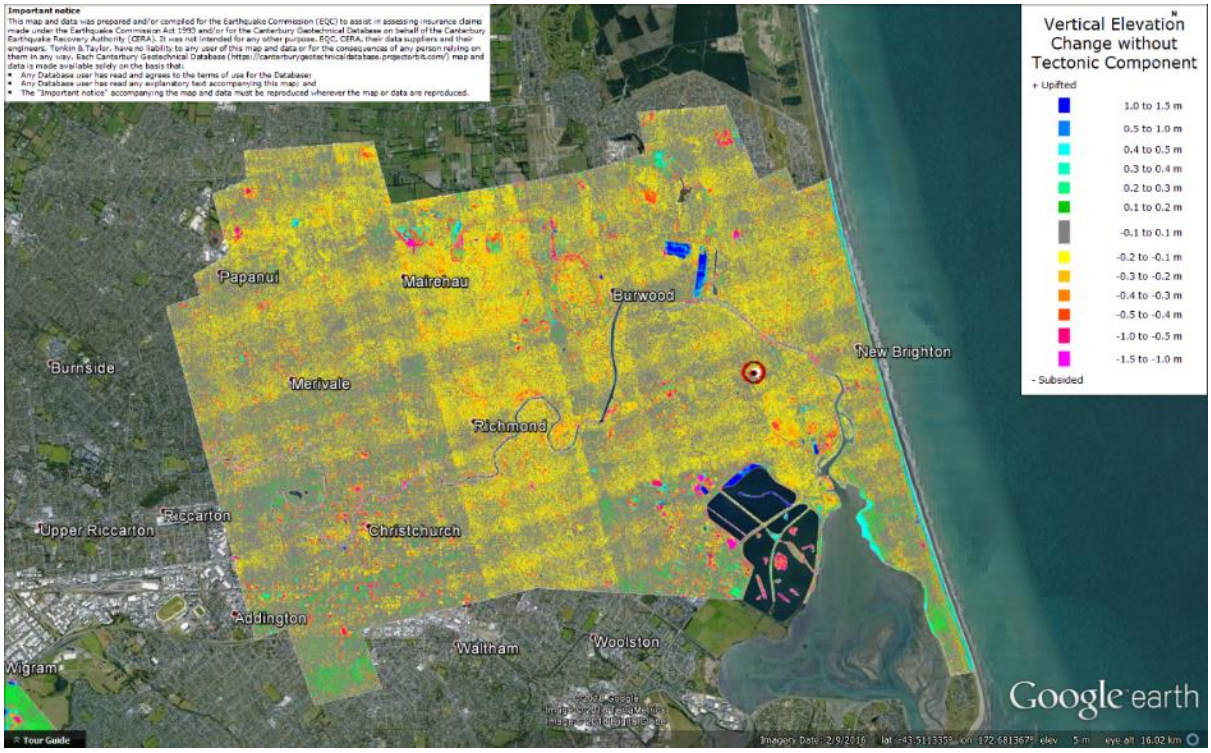

Figure 19: Vertical Ground Movements (Surface – Tectonic) for Sep 2010 Earthquake – the site is not in the apparent zone of overestimated ground surface subsidence.

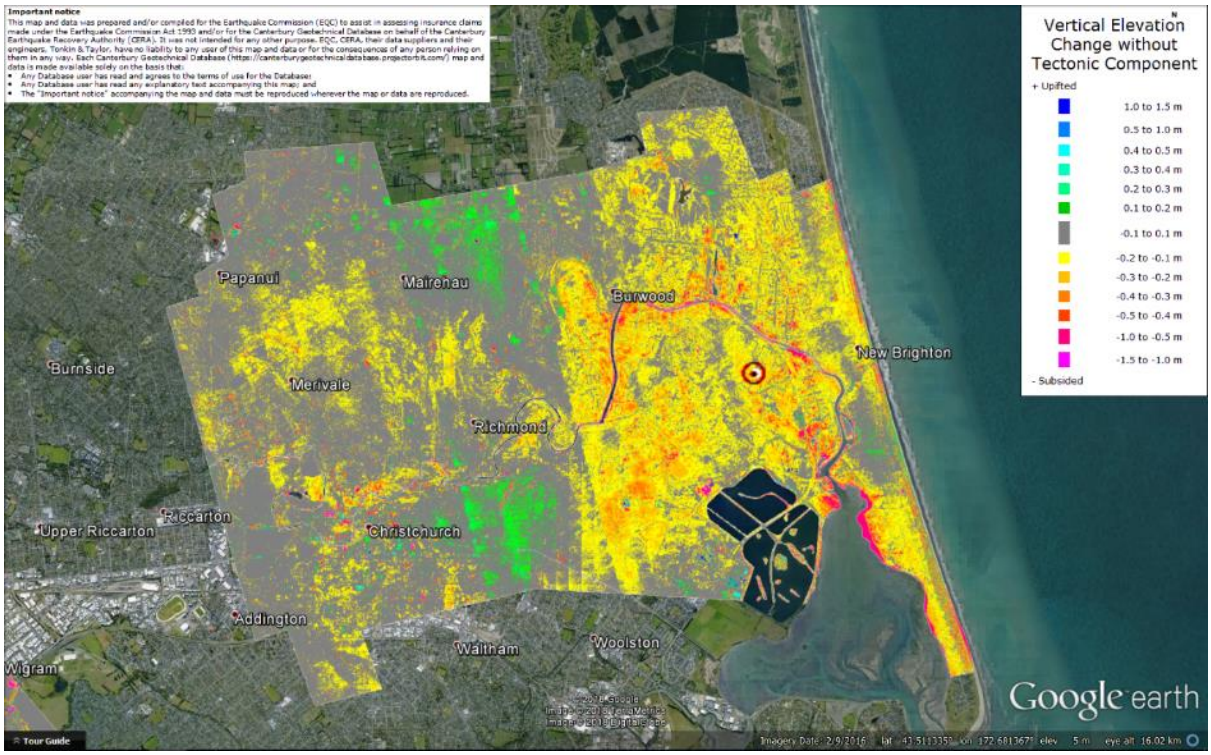

Figure 20: Vertical Ground Movements (Surface – Tectonic) for Feb 2011 Earthquake – the site is not in the apparent zone of underestimated ground surface subsidence.

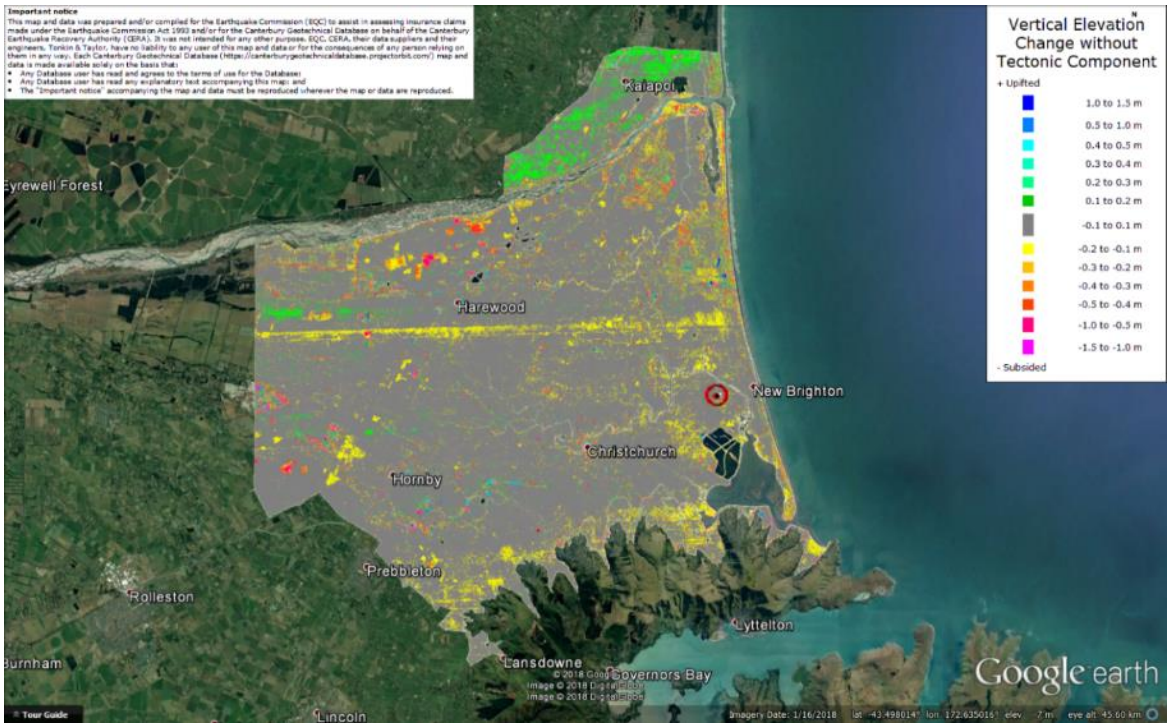

Figure 21: Vertical Ground Movements (Surface – Tectonic) for June 2011 Earthquake – the site is not in the apparent zone of overestimated or underestimated ground surface subsidence.

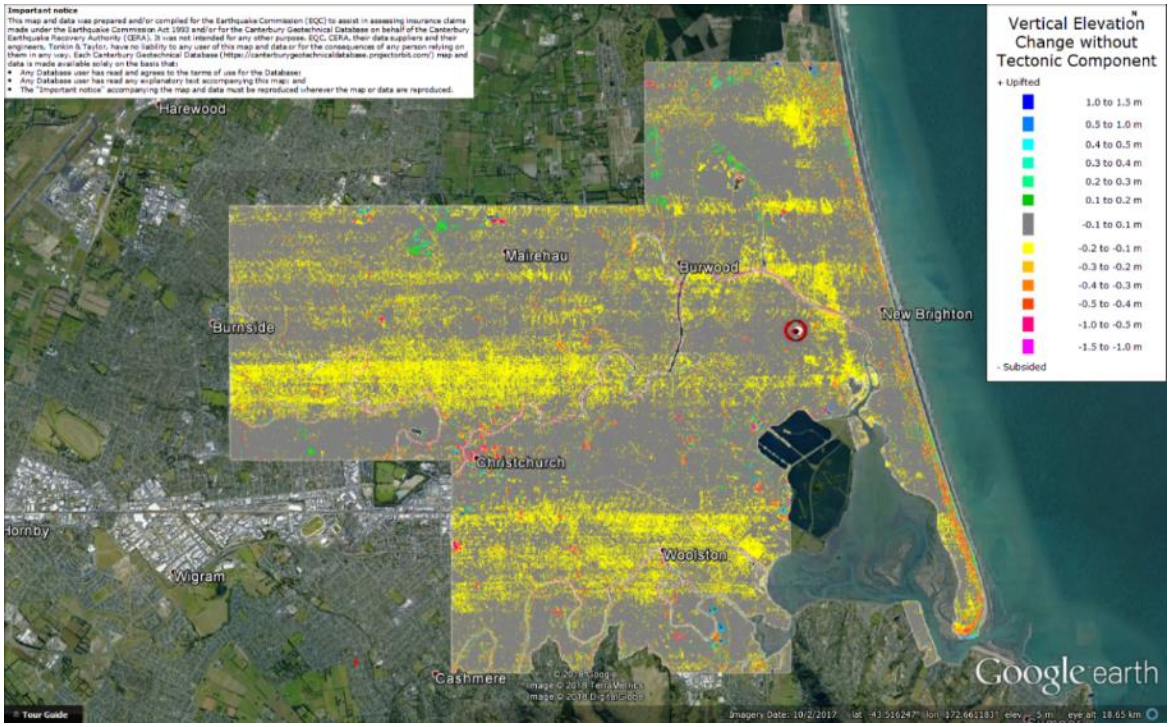

Figure 22: Vertical Ground Movements (Surface – Tectonic) for Dec 2011 Earthquake – the site is not in the apparent zone of overestimated or underestimated ground surface subsidence.

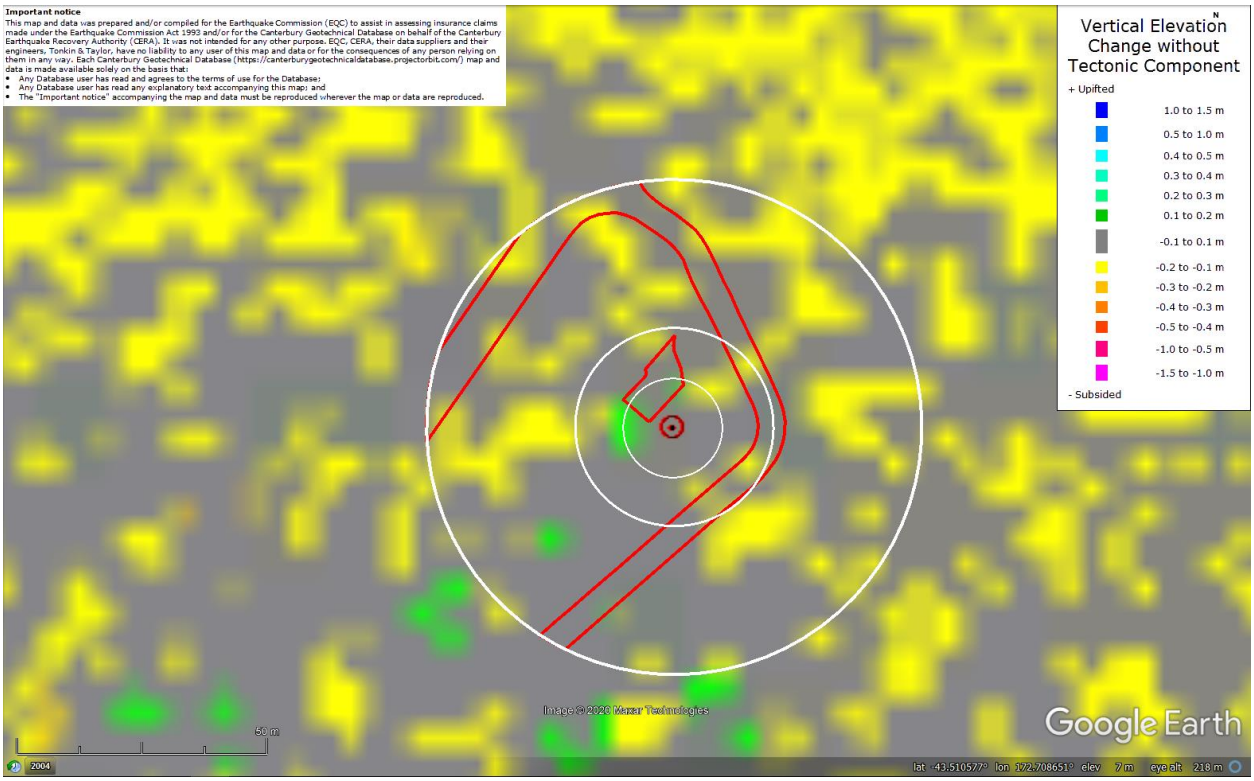

Figure 23: Ground surface subsidence without tectonic component for Sep 2010 Earthquake according to the LiDAR DEM.

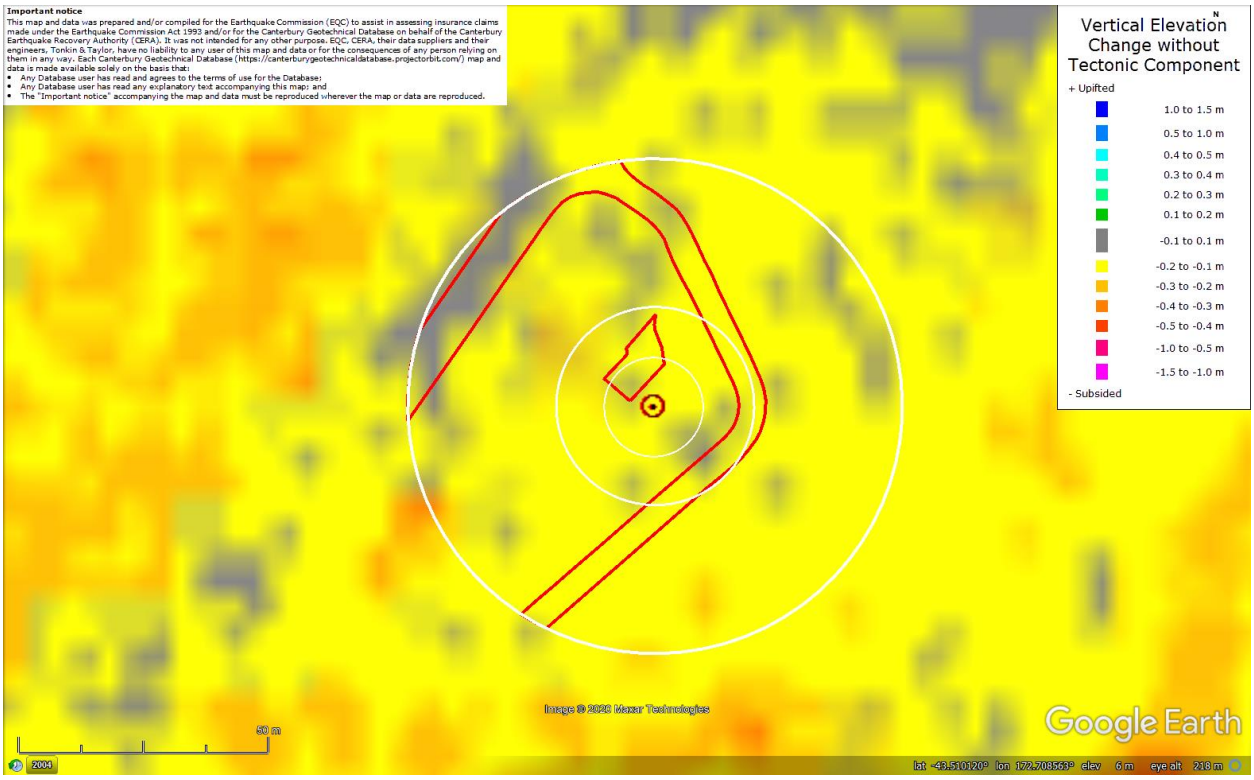

Figure 24: Ground surface subsidence without tectonic component for Feb 2011 Earthquake according to the LiDAR DEM.

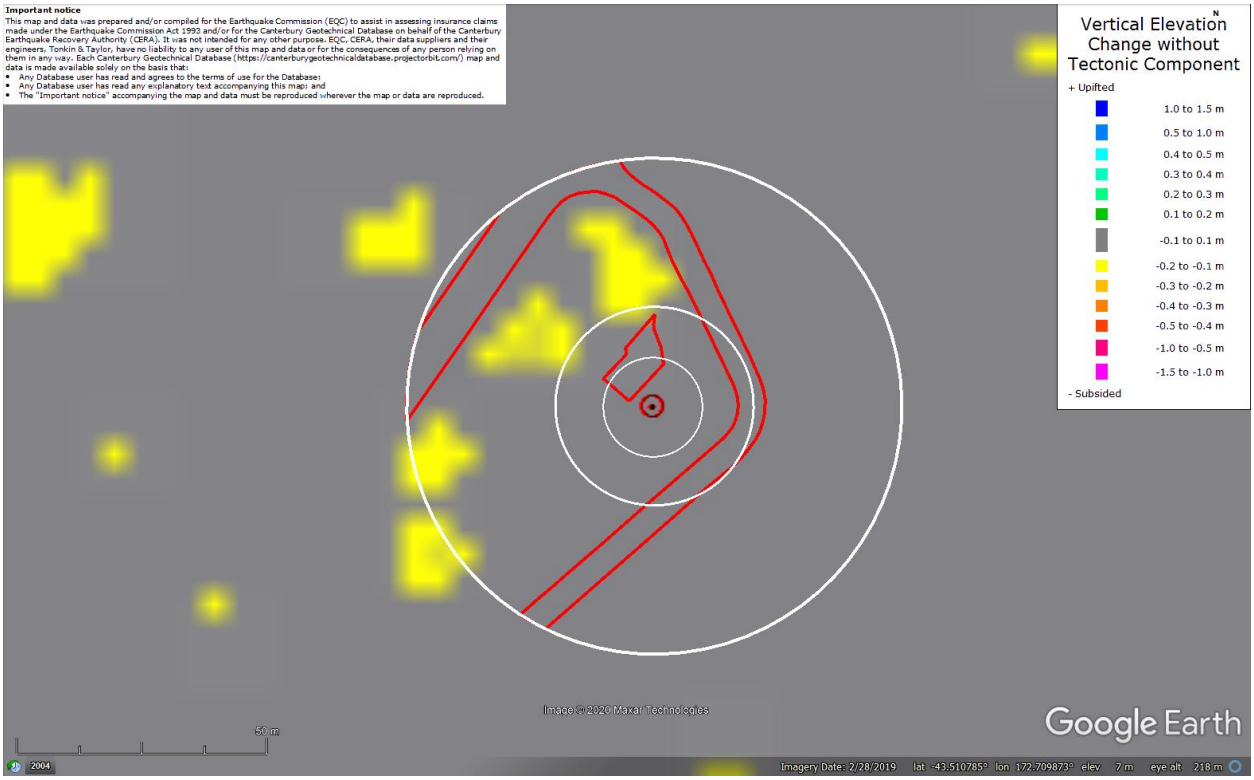

Figure 25: Ground surface subsidence without tectonic component for June 2011 Earthquake according to the LiDAR DEM.

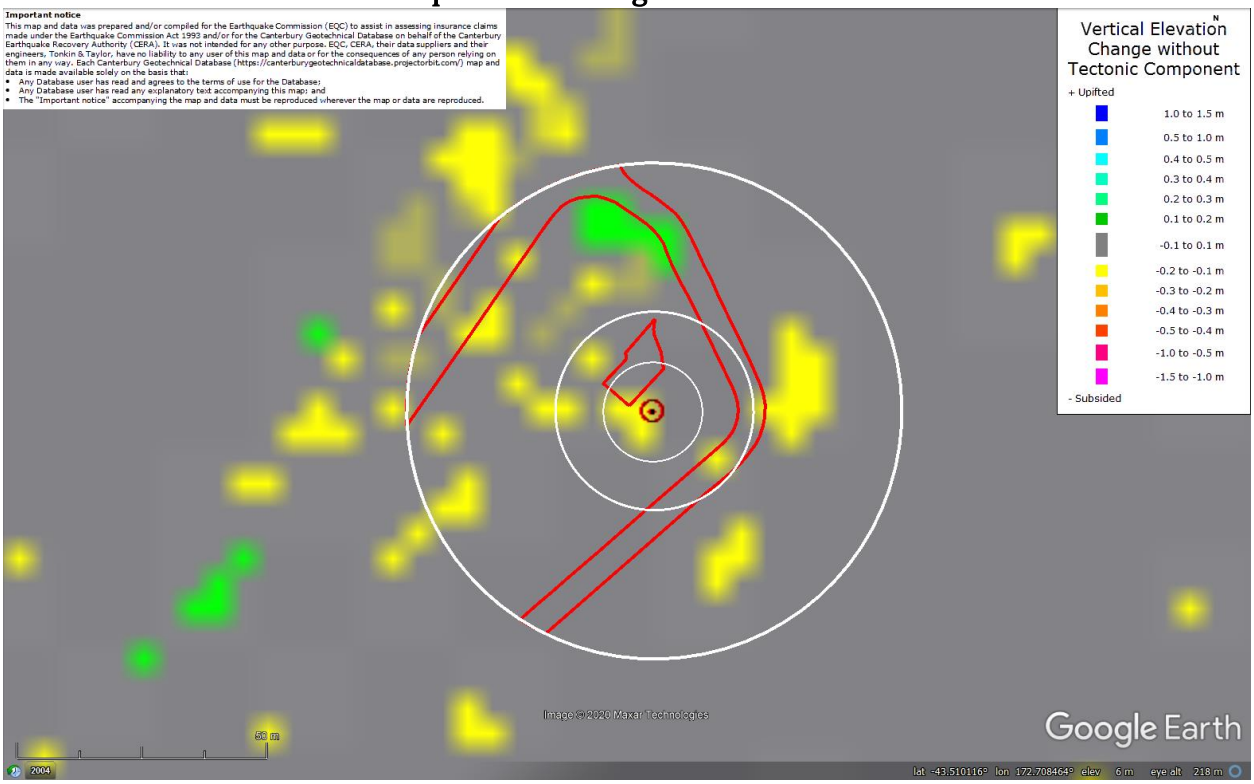

Figure 26: Ground surface subsidence without tectonic component for Dec 2011 Earthquake according to the LiDAR DEM.

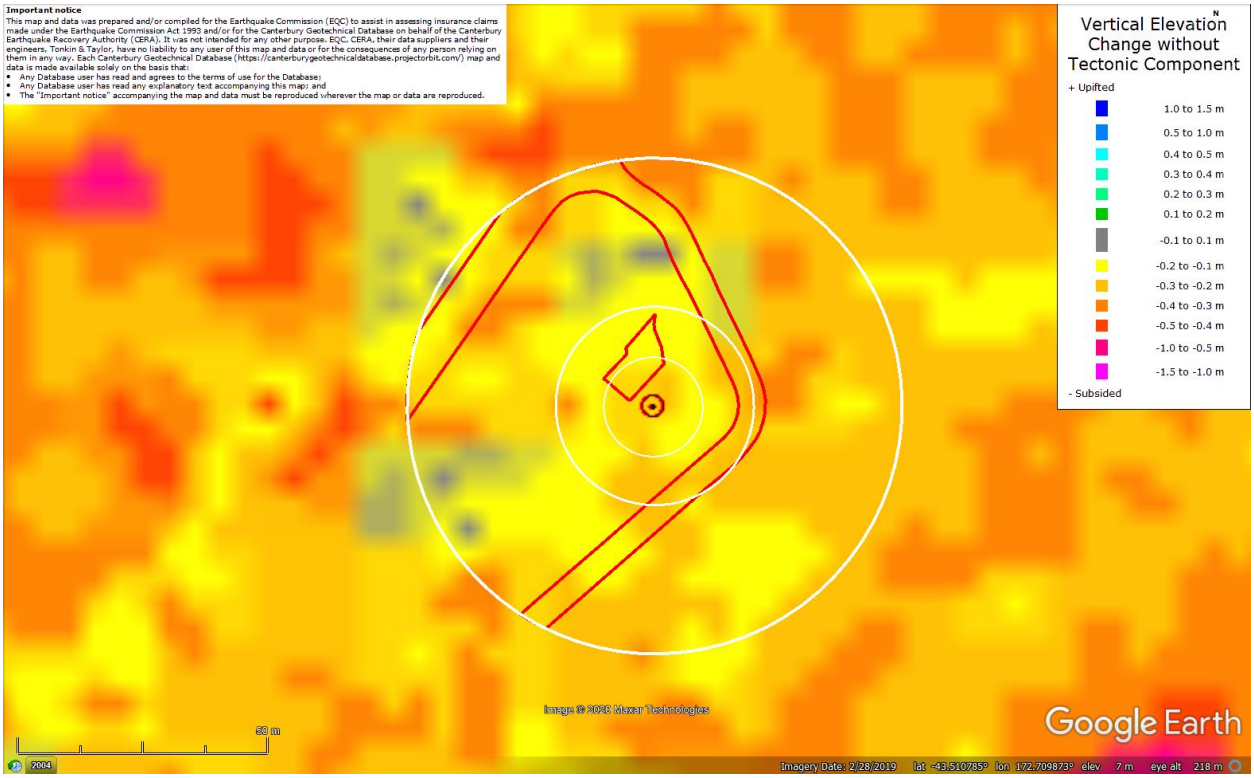

Figure 27: Ground surface subsidence without tectonic component for Canterbury Earthquake Sequence according to the LiDAR DEM.

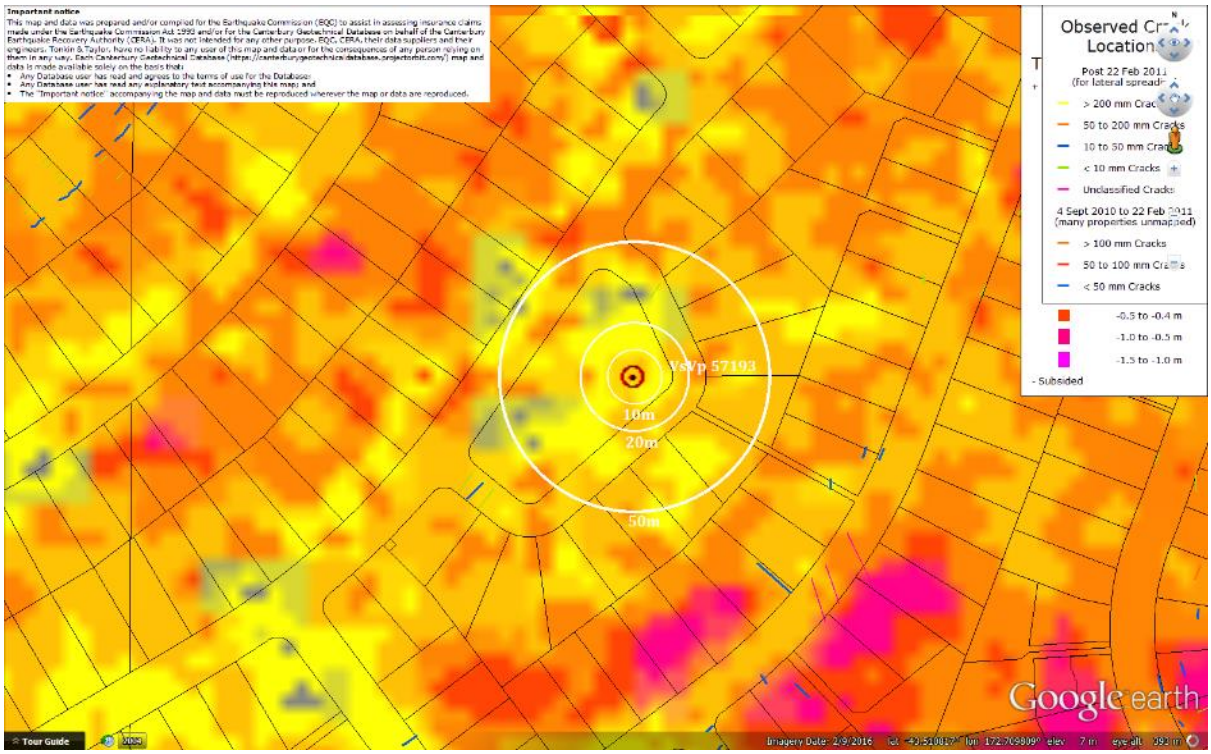

Figure 28: Absence of significant ground cracks indicating no lateral spreading for Canterbury Earthquake Sequence.

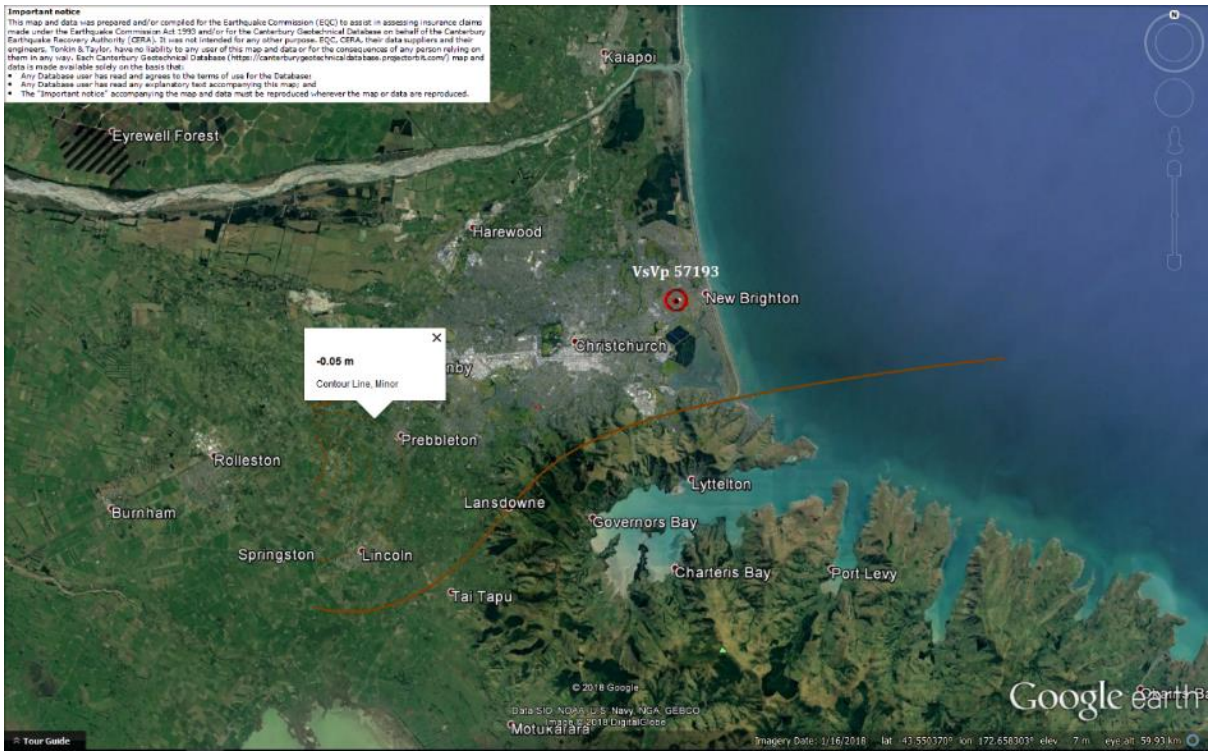

Figure 29: Vertical tectonic movements for Sep 2010 Earthquake.

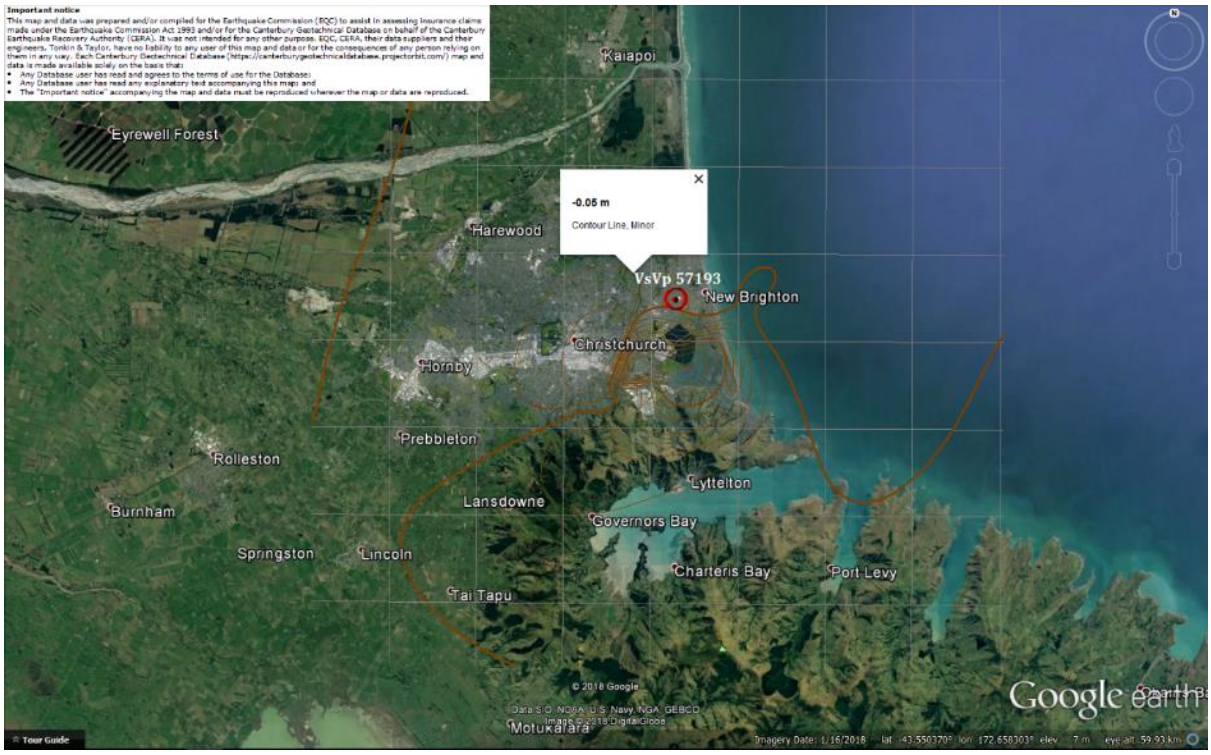

Figure 30: Vertical tectonic movements for Feb 2011 Earthquake.

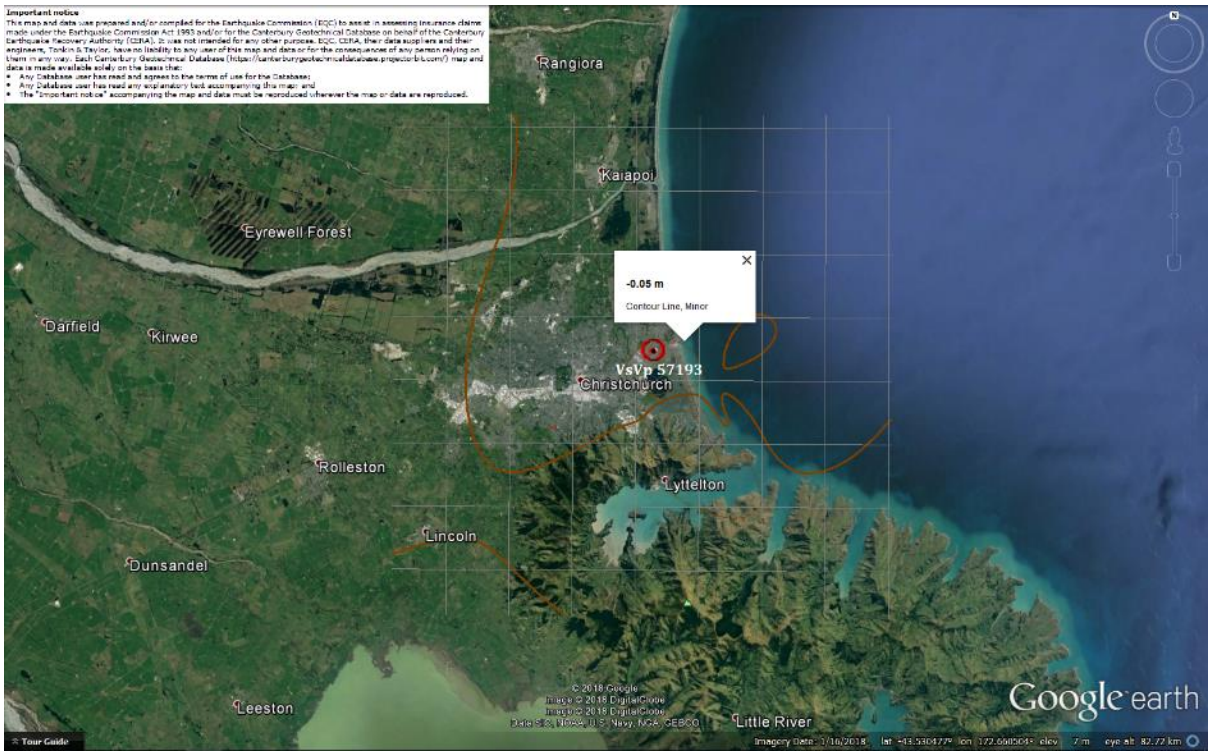

Figure 31: Vertical tectonic movements for June 2011 Earthquake.

Figure 32: Vertical tectonic movements for Dec 2011 Earthquake.

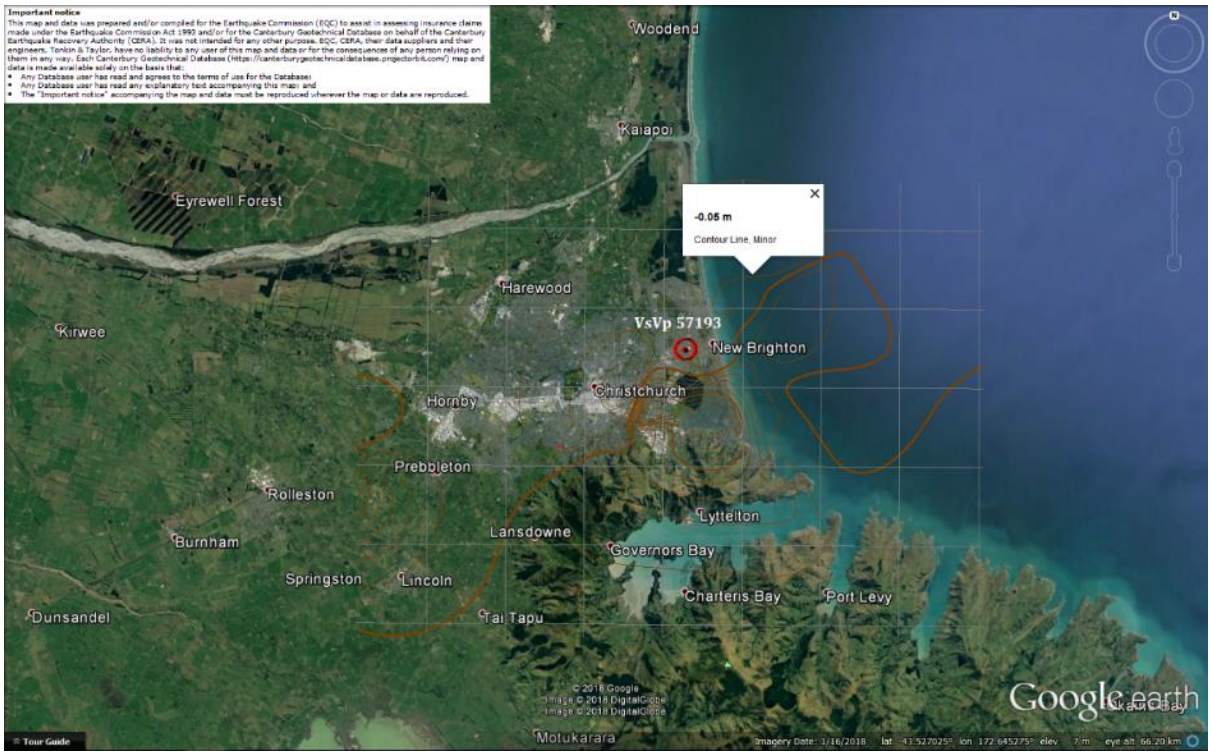

Figure 33: Vertical tectonic movements for Canterbury Earthquake Sequence.

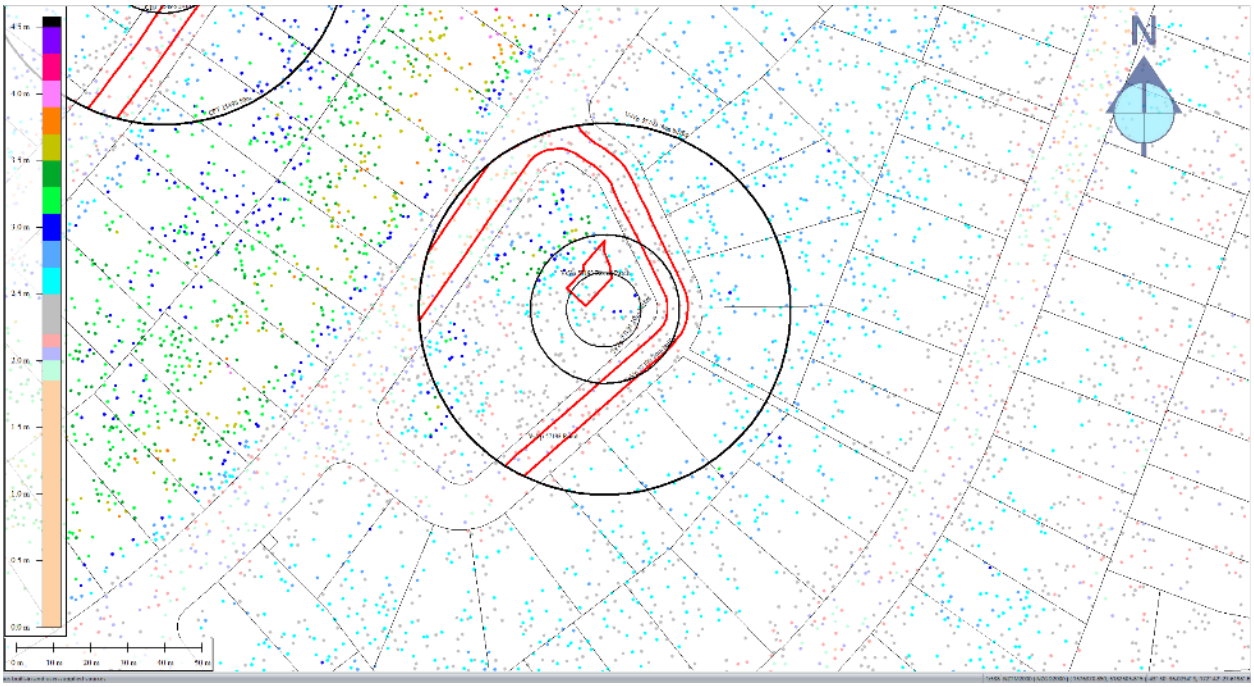

Figure 34: Jul 2003 LiDAR survey.

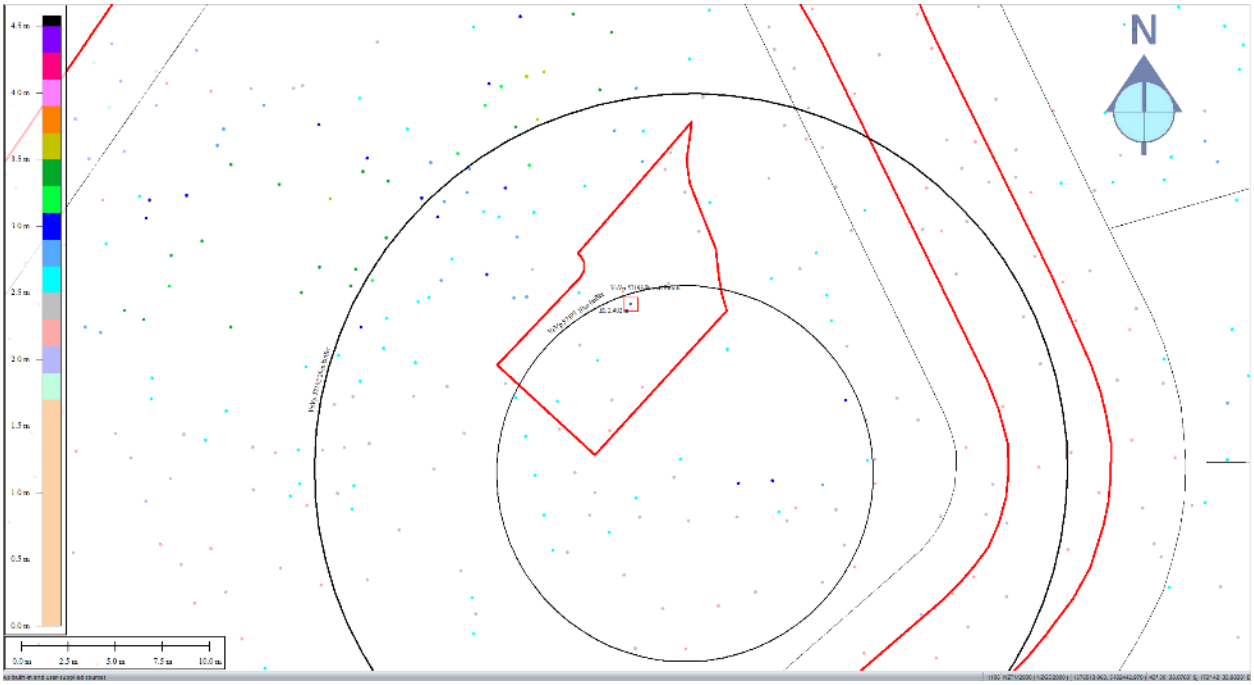

Figure 35: Ground surface elevation averaged over Paved Patch for Jul 2003 LiDAR survey.

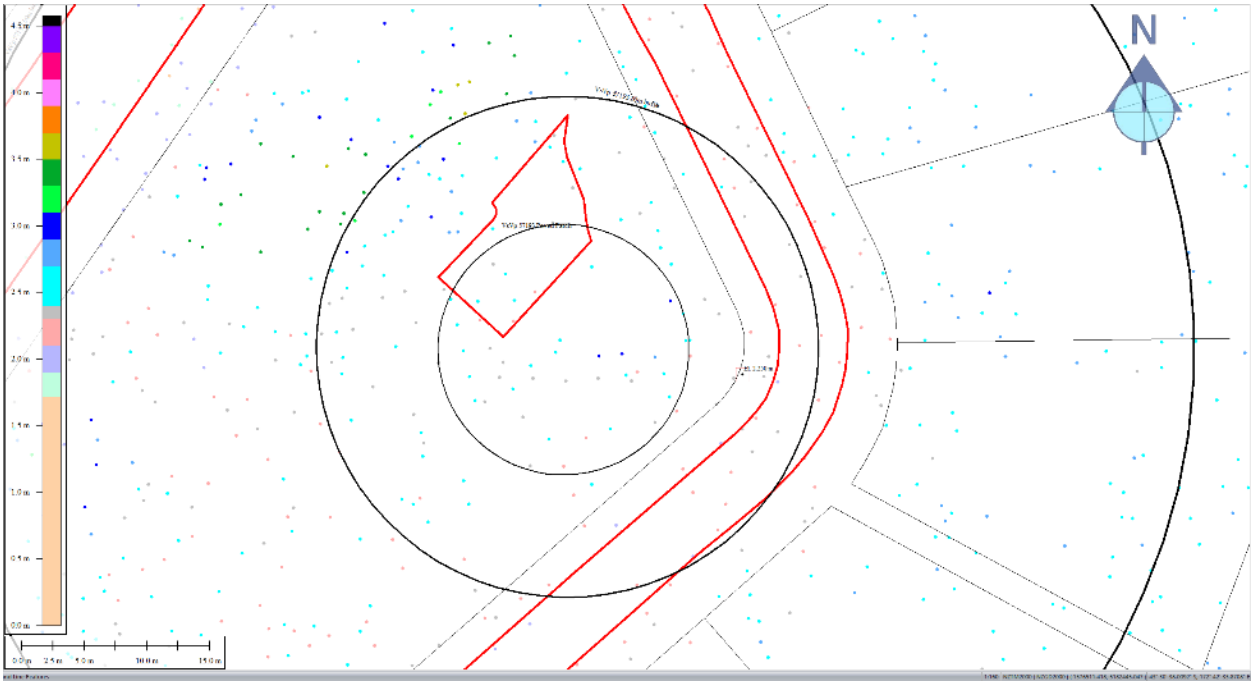

Figure 36: Ground surface elevation averaged over the 20-m buffer for Road for Jul 2003 LiDAR survey.

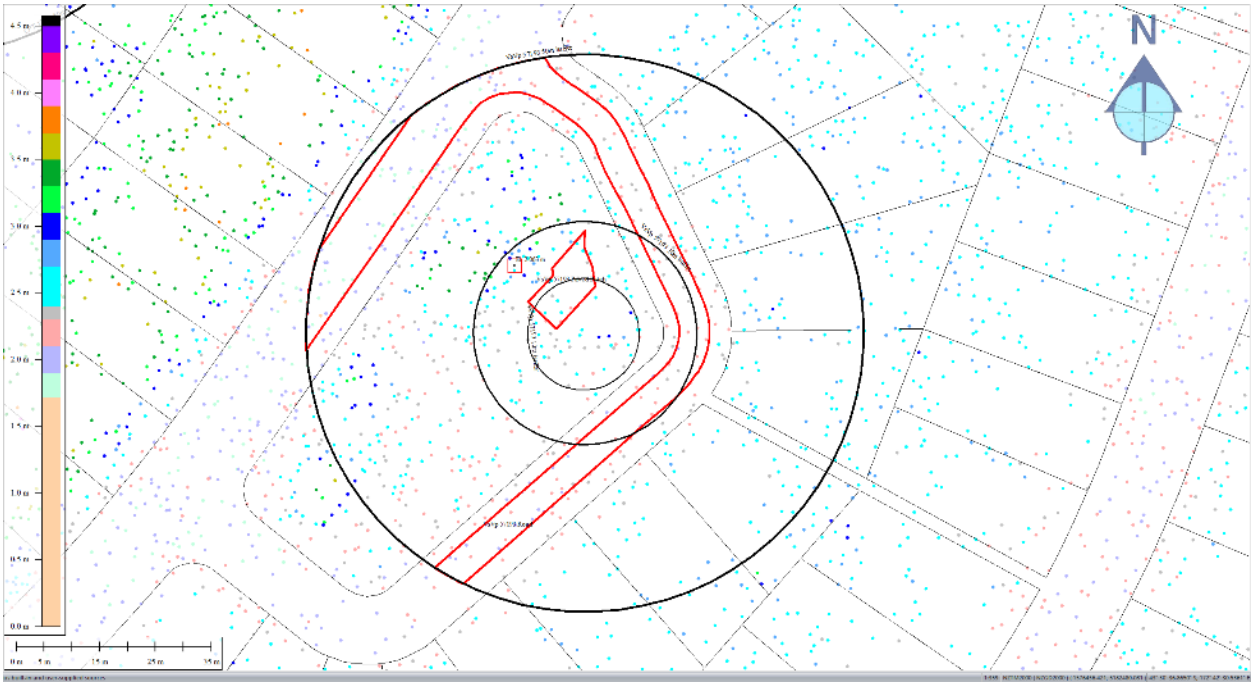

Figure 37: Ground surface elevation averaged over the 50-m buffer for Road for Jul 2003 LiDAR survey.

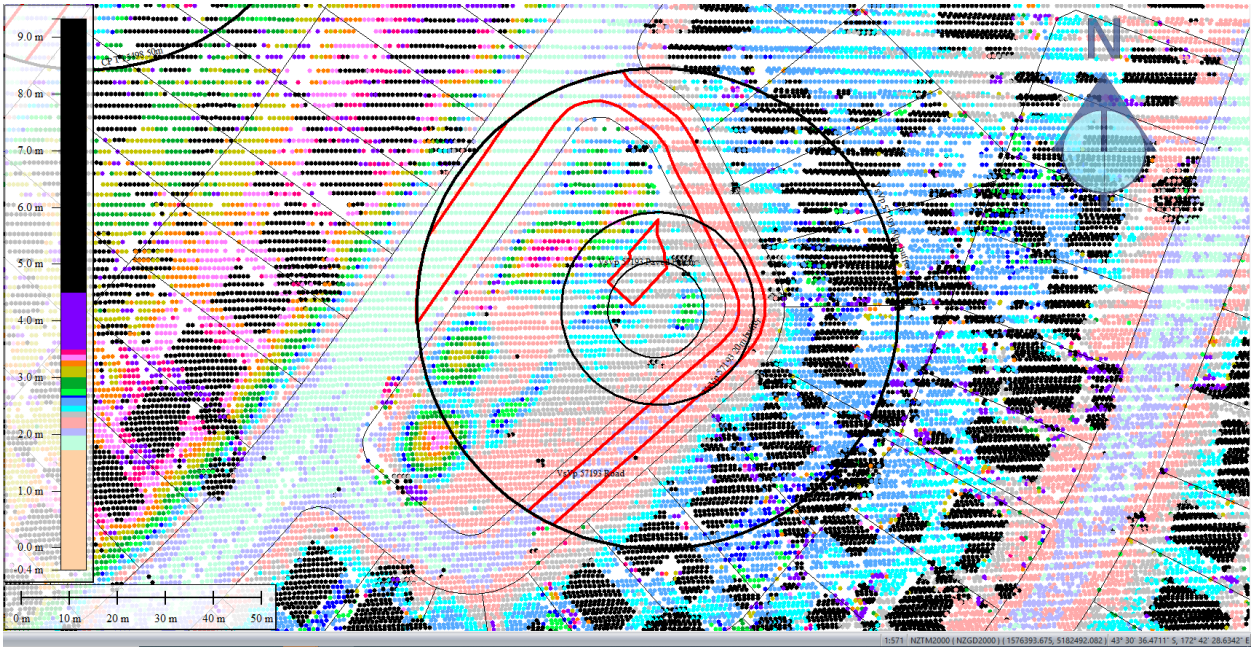

Figure 38: Sep 5, 2010 LiDAR survey.

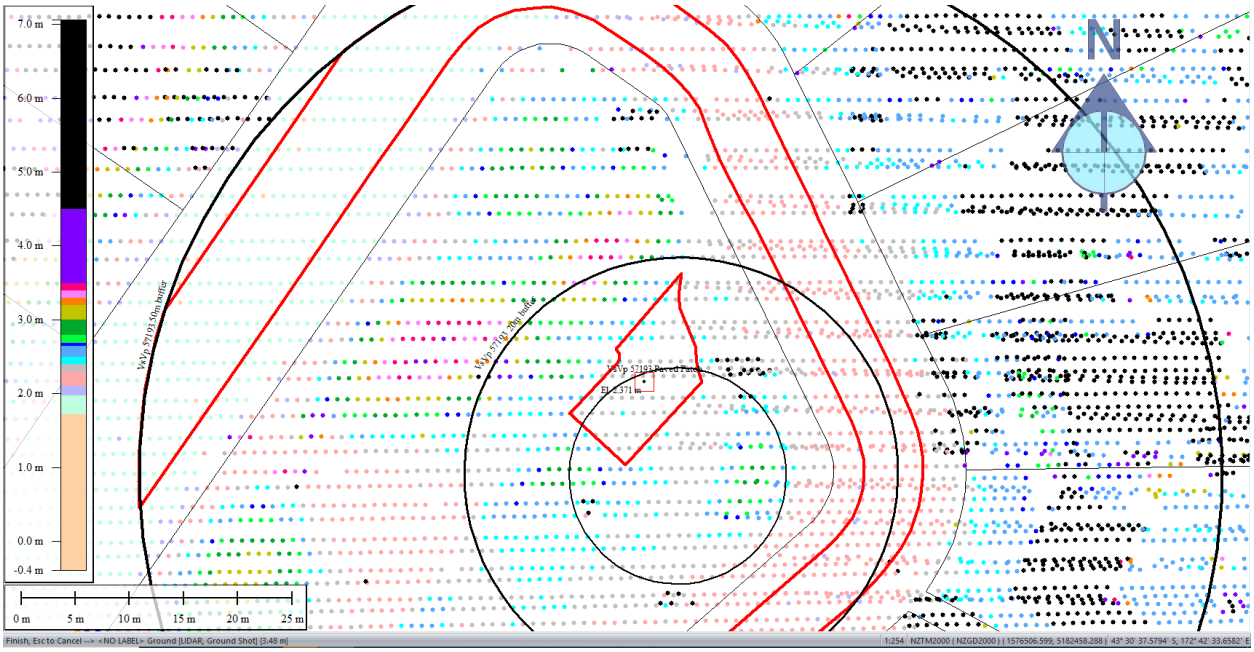

Figure 39: Ground surface elevation averaged over Paved Patch for Sep 5, 2010 LiDAR survey.

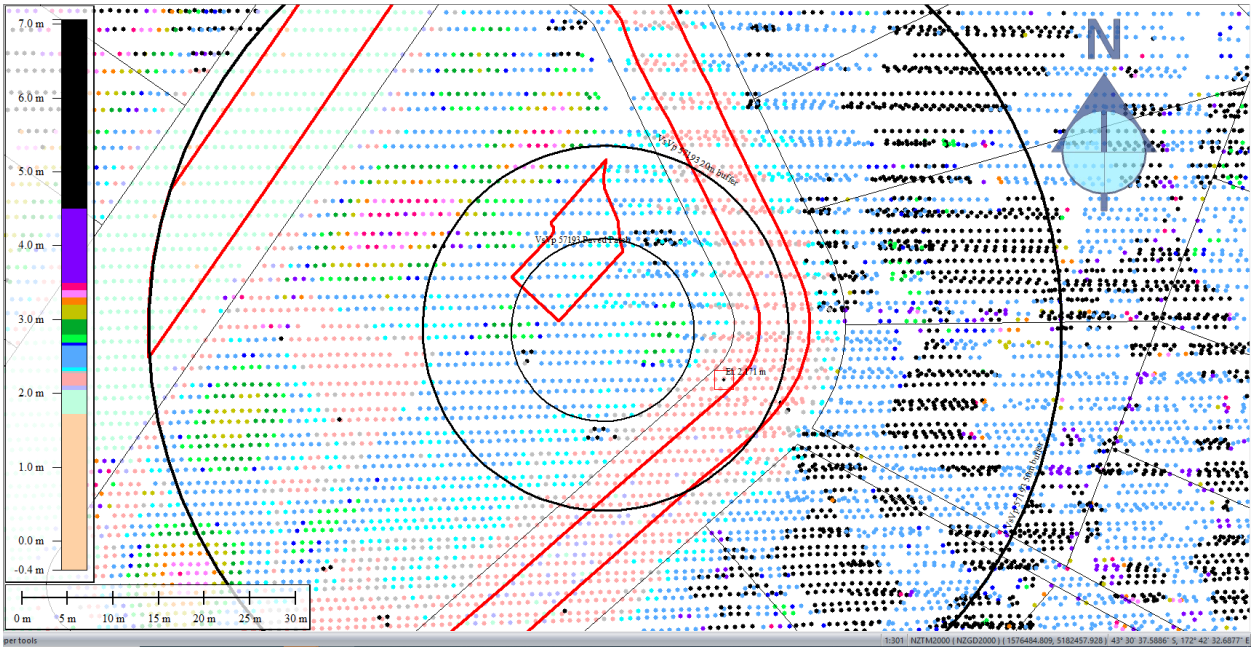

Figure 40: Ground surface elevation averaged over the 20-m buffer for Road for Sep 5, 2010 LiDAR survey.

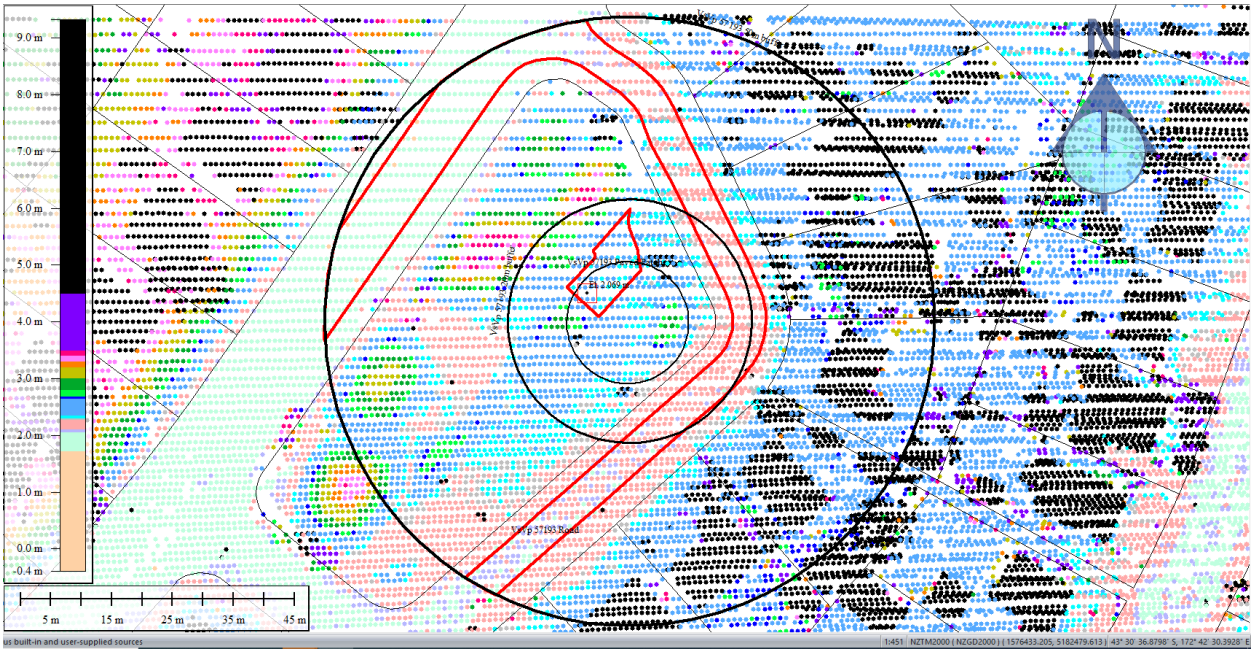

Figure 41: Ground surface elevation averaged over the 50-m buffer for Road for Sep 5, 2010 LiDAR survey.

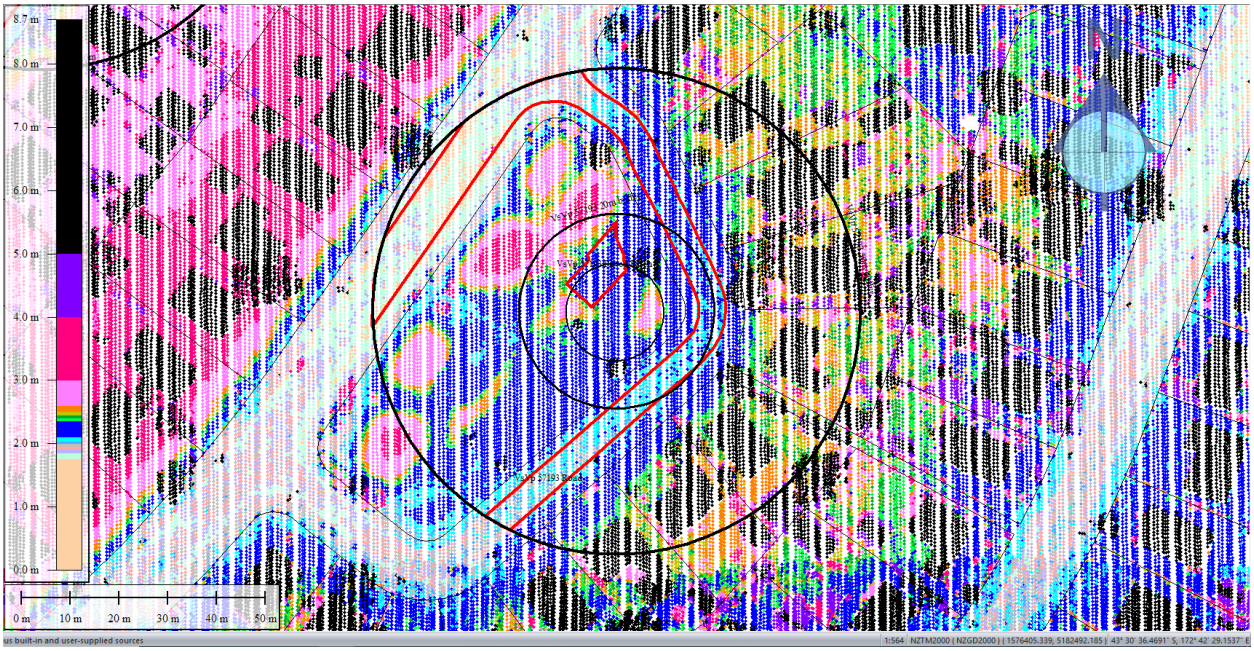

Figure 42: Mar 2011 LiDAR survey.

Figure 43: Ground surface elevation averaged over Paved Patch for Mar 2011 LiDAR survey.

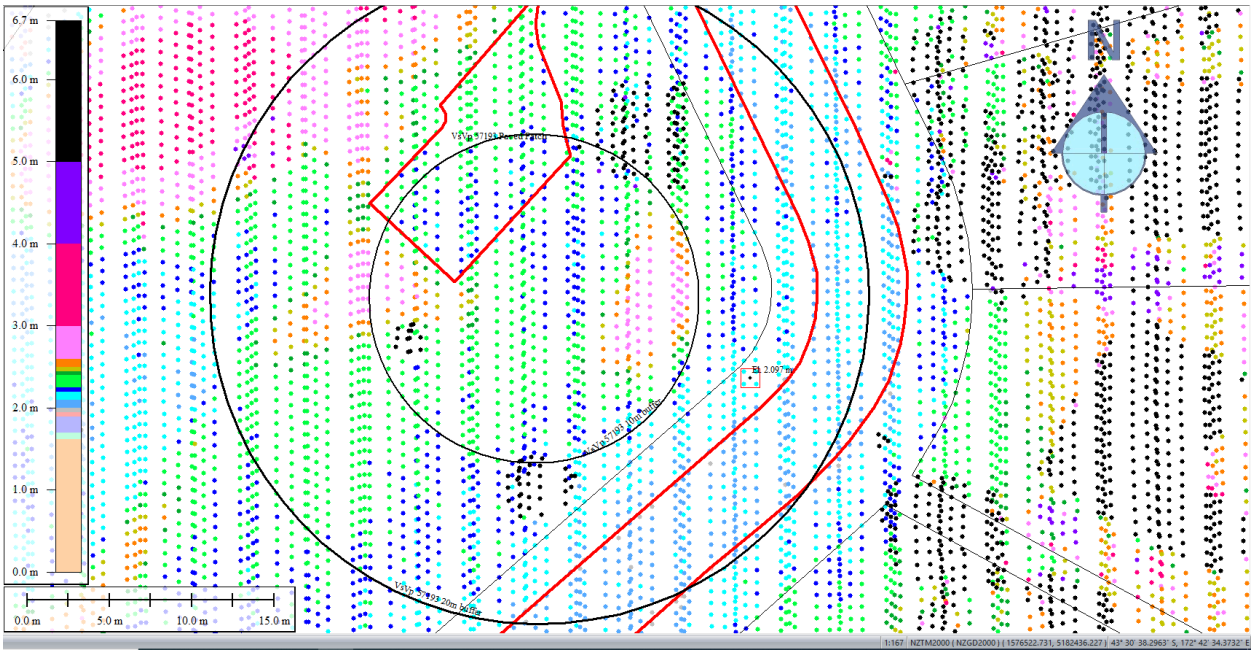

Figure 44: Ground surface elevation averaged over the 20-m buffer for Road for Mar 2011 LiDAR survey.

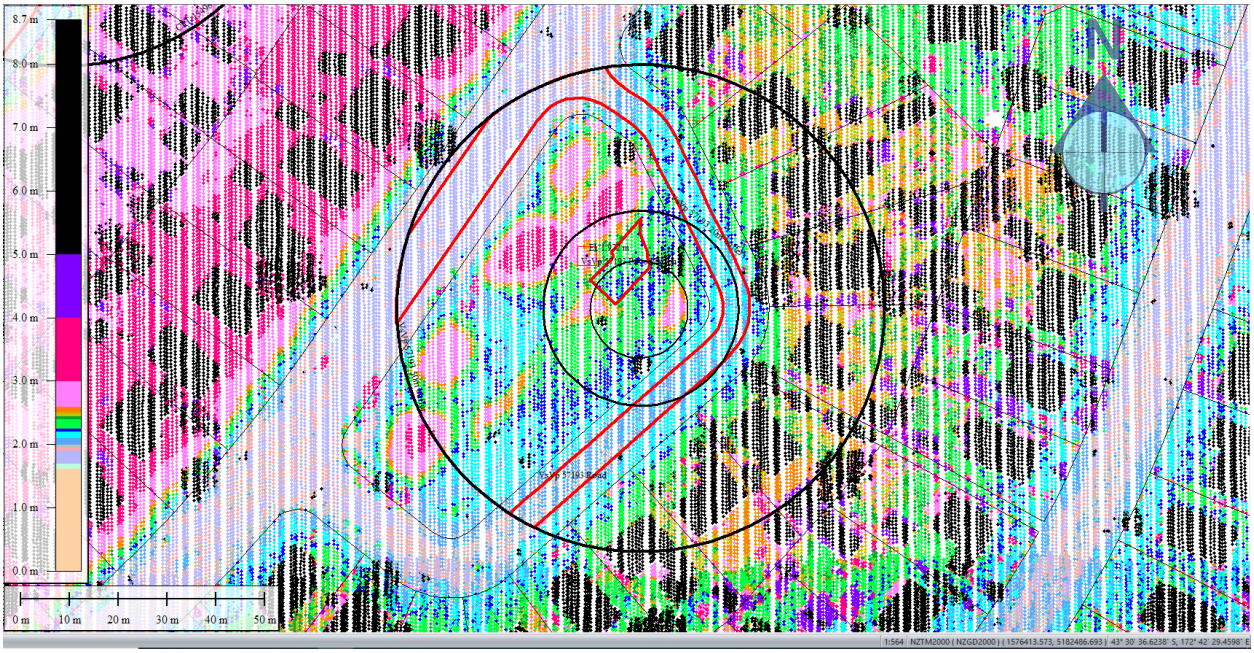

Figure 45: Ground surface elevation averaged over the 50-m buffer for Road for Mar 2011 LiDAR survey.

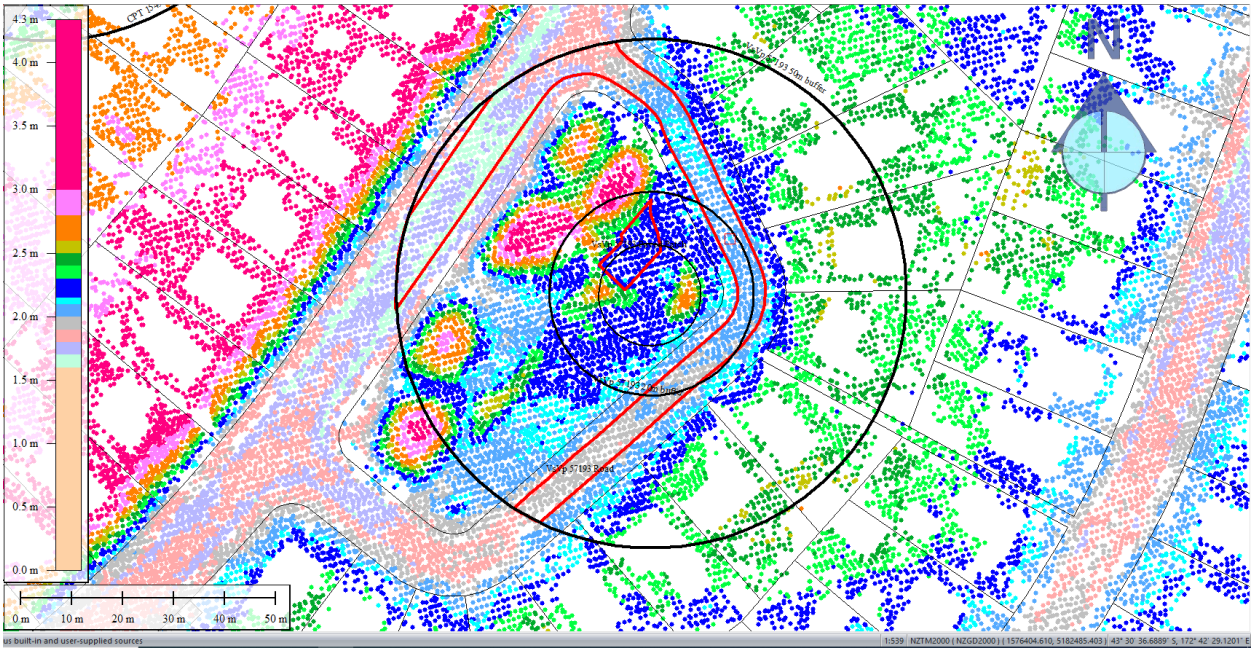

Figure 46: May 2011 LiDAR survey.

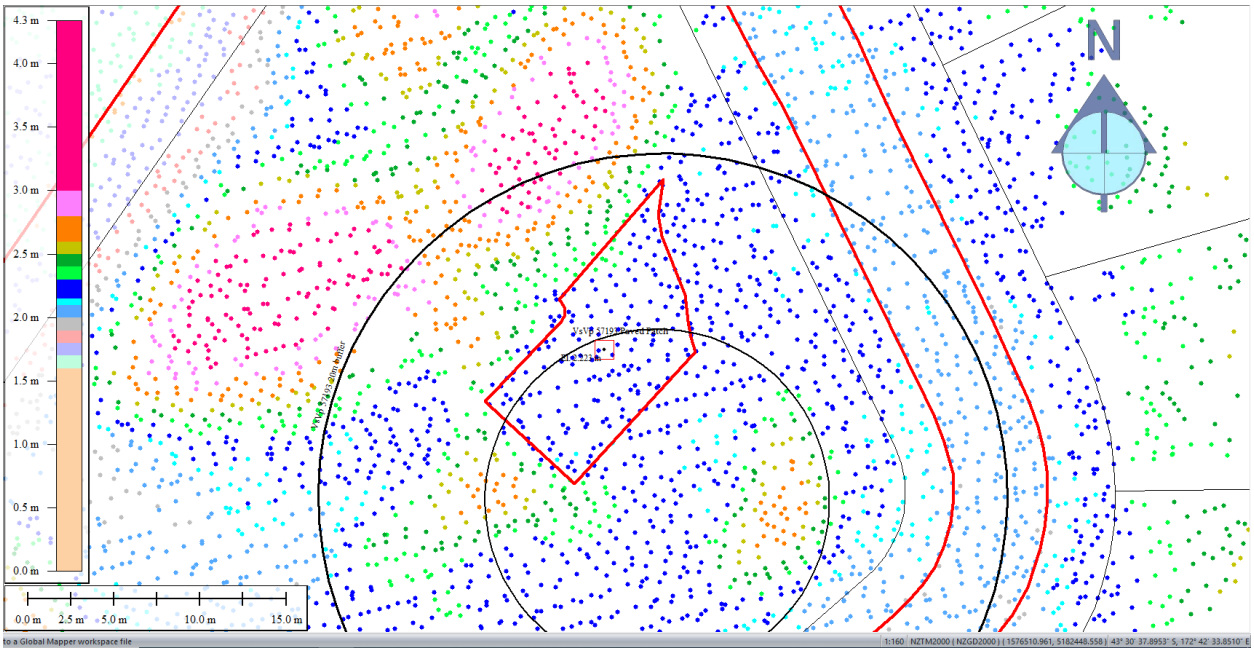

Figure 47: Ground surface elevation averaged over Paved Patch for May 2011 LiDAR survey.

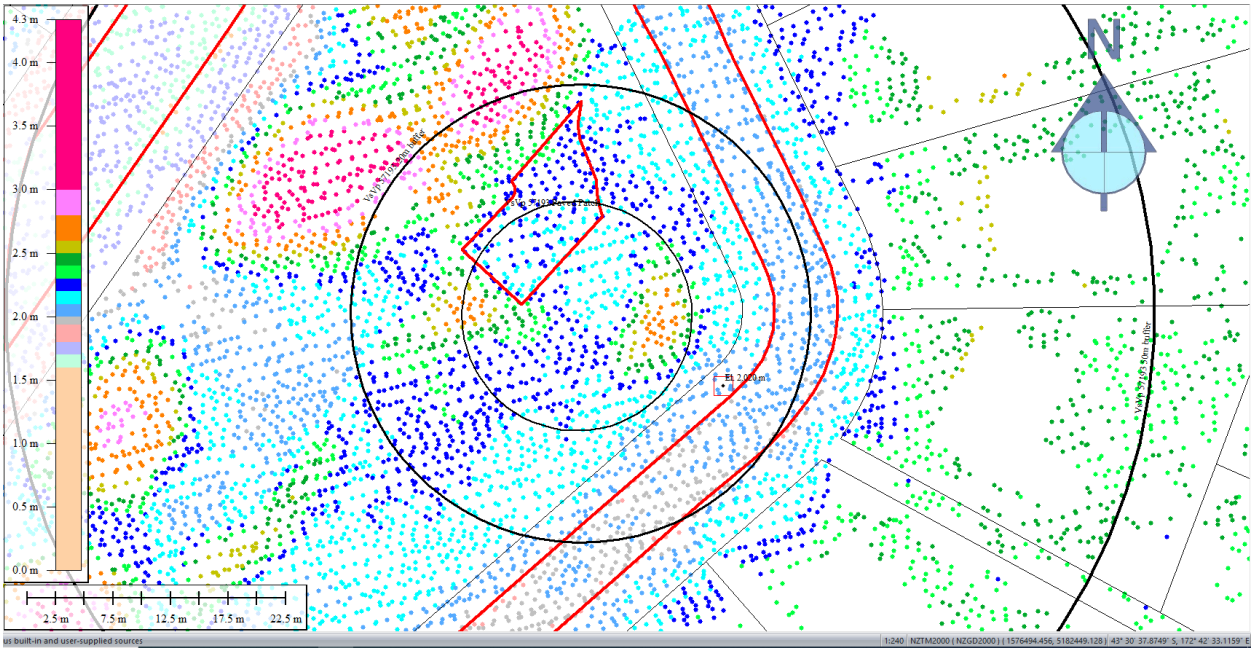

Figure 48: Ground surface elevation averaged over the 20-m buffer for Road for May 2011 LiDAR survey.

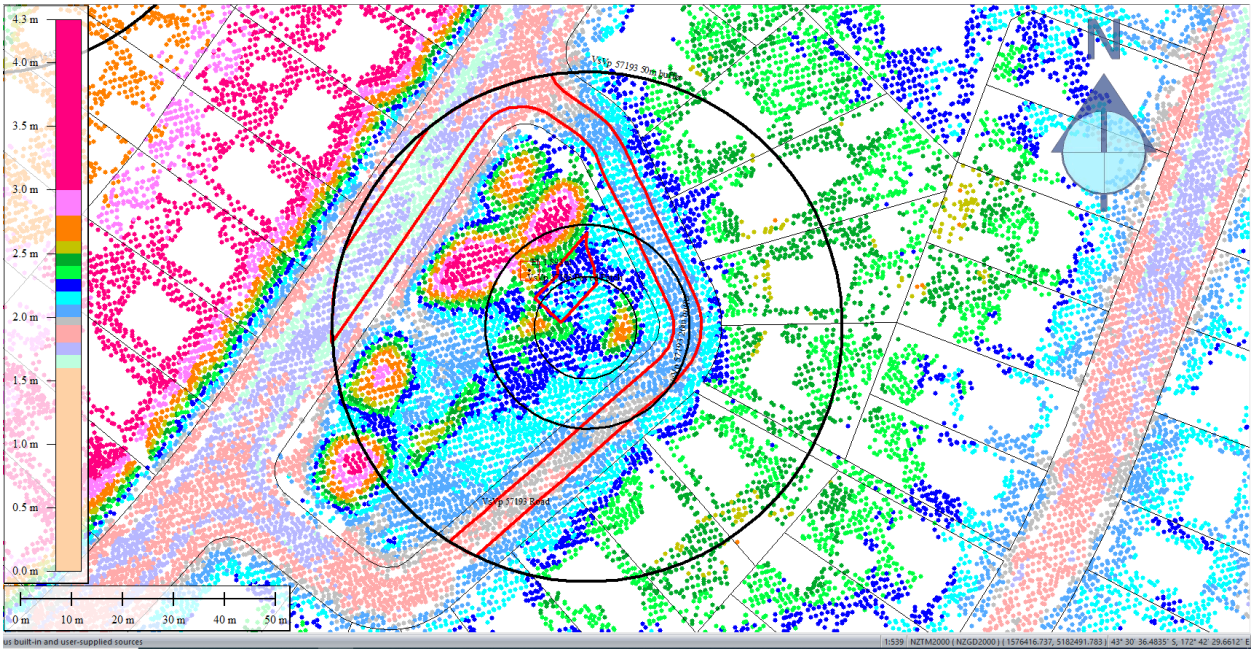

Figure 49: Ground surface elevation averaged over the 50-m buffer for Road for May 2011 LiDAR survey.

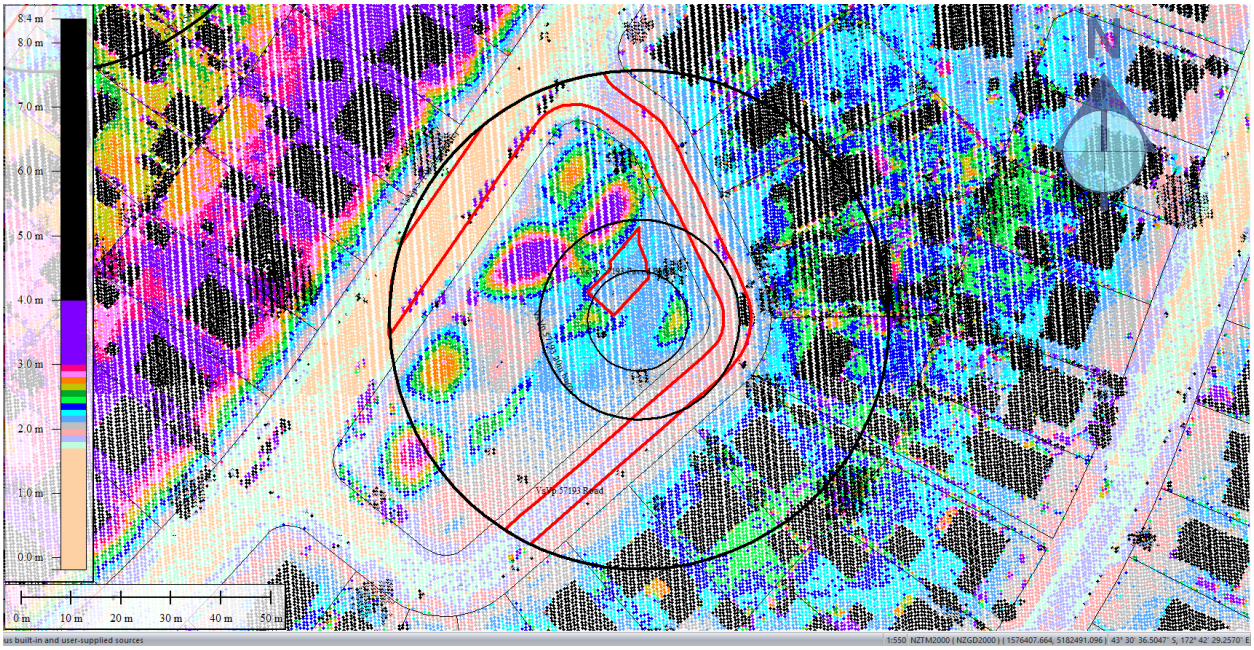

Figure 50: Sep 2011 LiDAR survey.

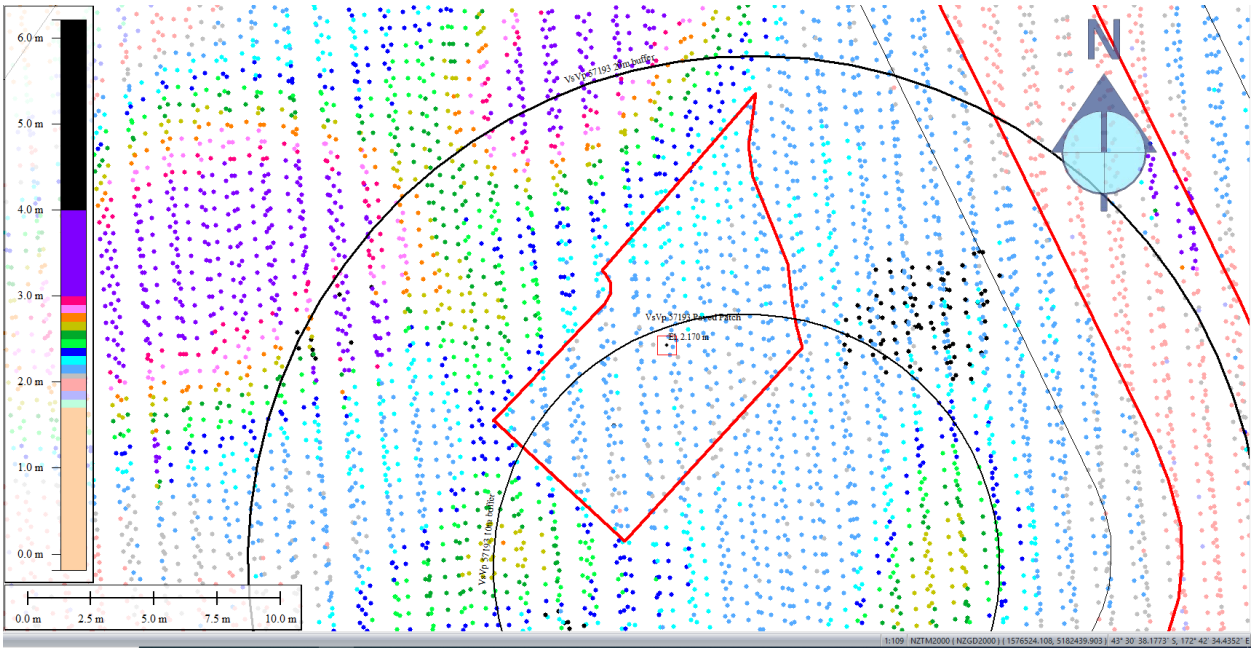

Figure 51: Ground surface elevation averaged over Paved Patch for Sep 2011 LiDAR survey.

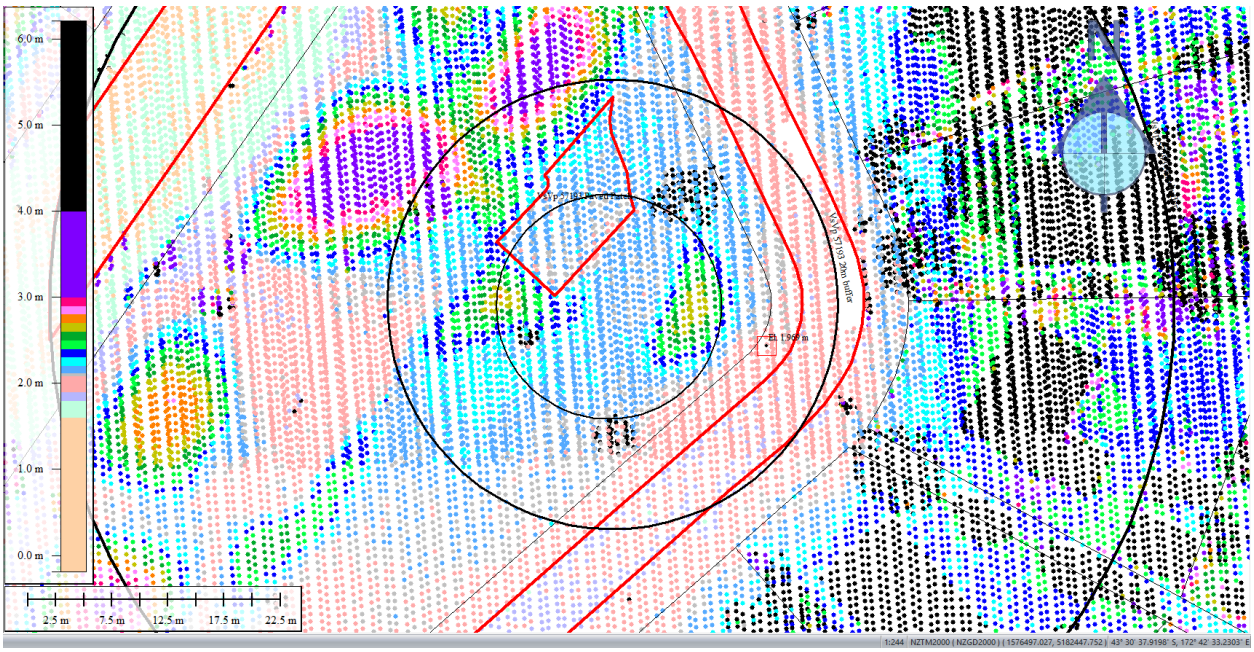

Figure 52: Ground surface elevation averaged over the 20-m buffer for Road for Sep 2011 LiDAR survey.

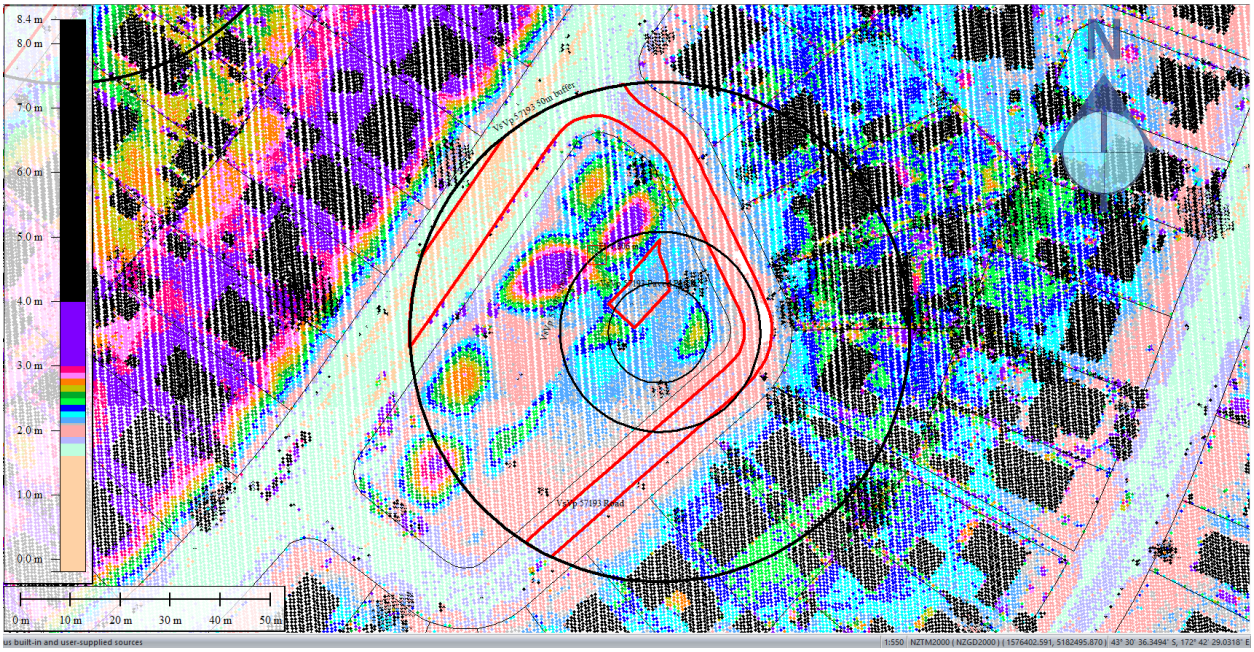

Figure 53: Ground surface elevation averaged over the 50-m buffer for Road for Sep 2011 LiDAR survey.

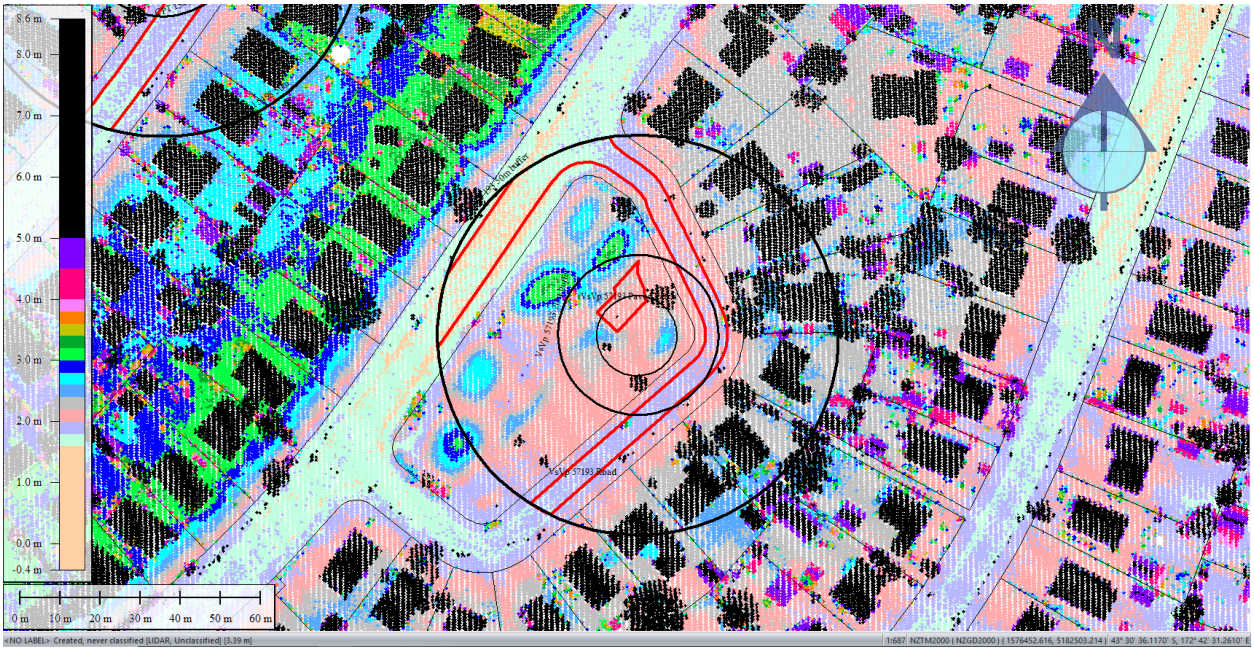

Figure 54: Feb 2012 LiDAR survey.

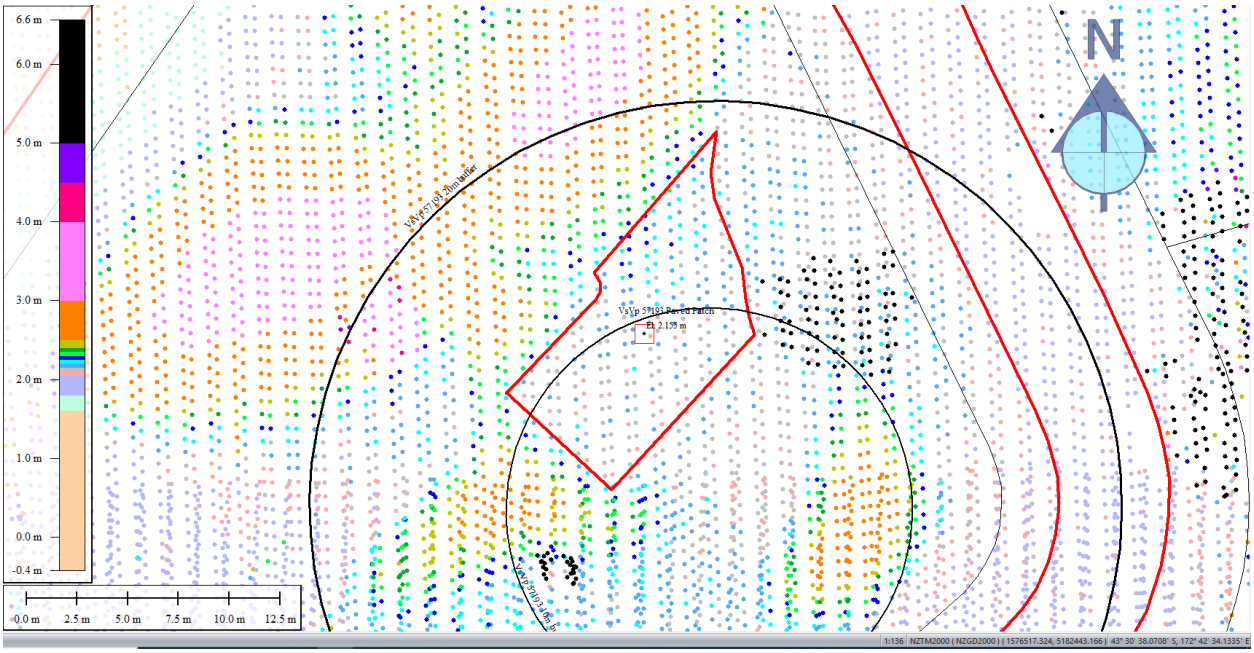

Figure 55: Ground surface elevation averaged over Paved Patch for Feb 2012 LiDAR survey.

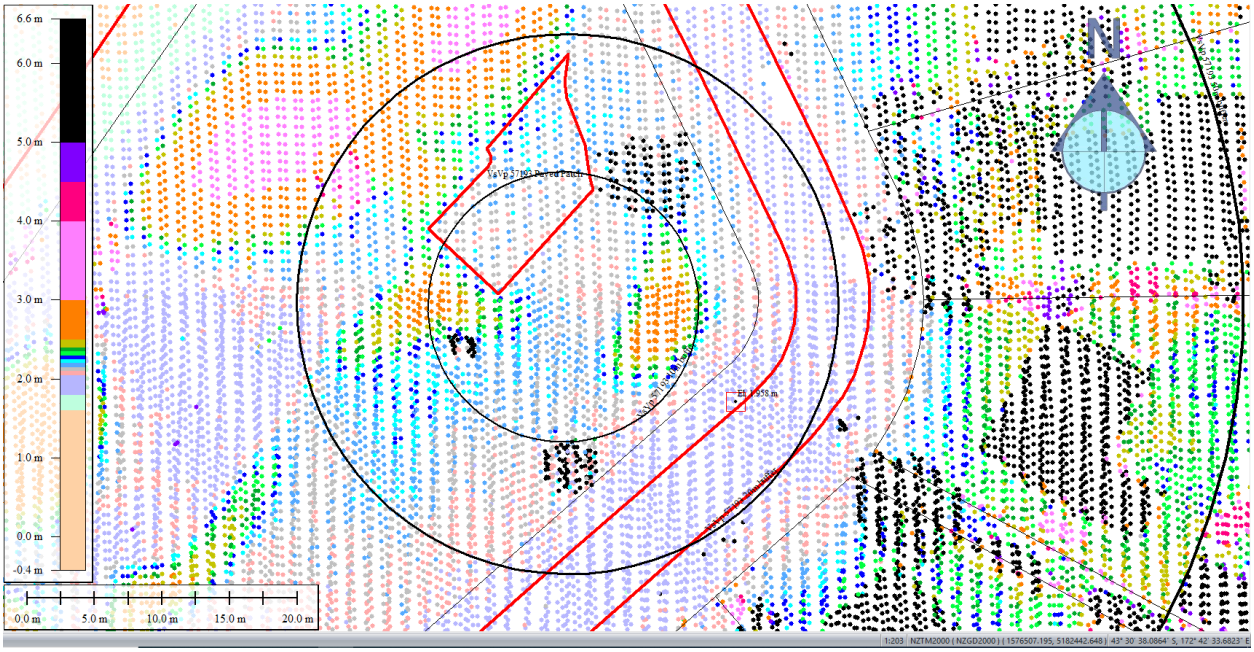

Figure 56: Ground surface elevation averaged over the 20-m buffer for Road for Feb 2012 LiDAR survey.

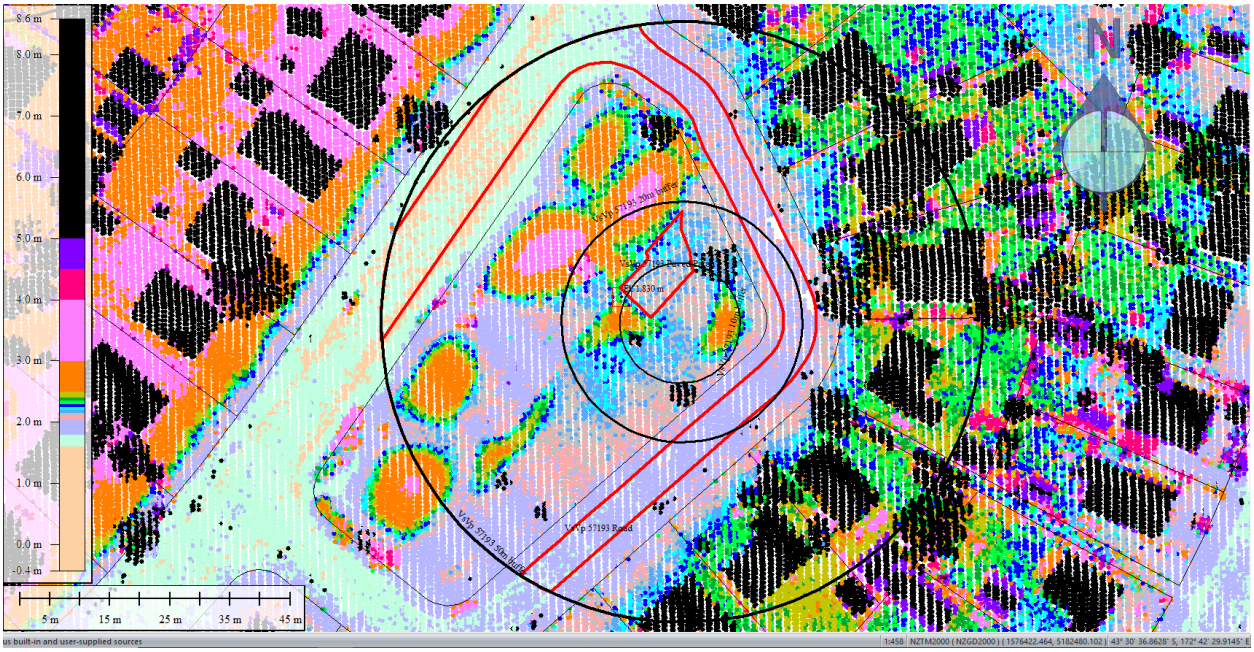

Figure 57: Ground surface elevation averaged over the 50-m buffer for Road for Feb 2012 LiDAR survey.

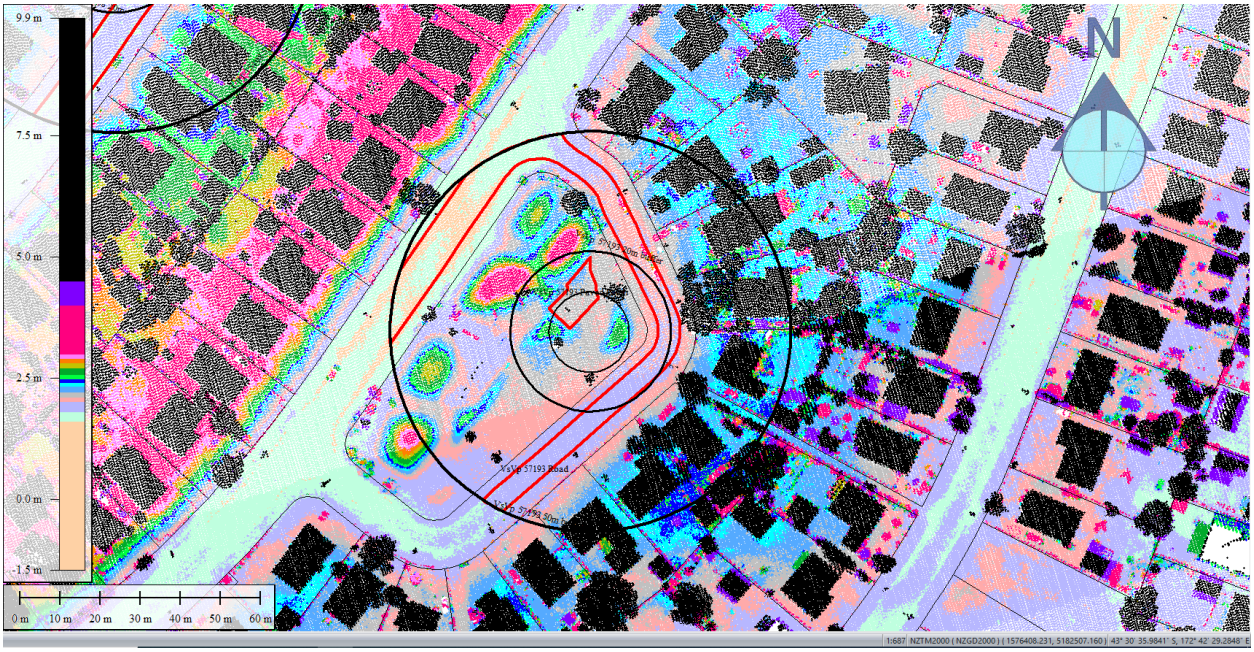

Figure 58: Oct 2015 LiDAR survey.

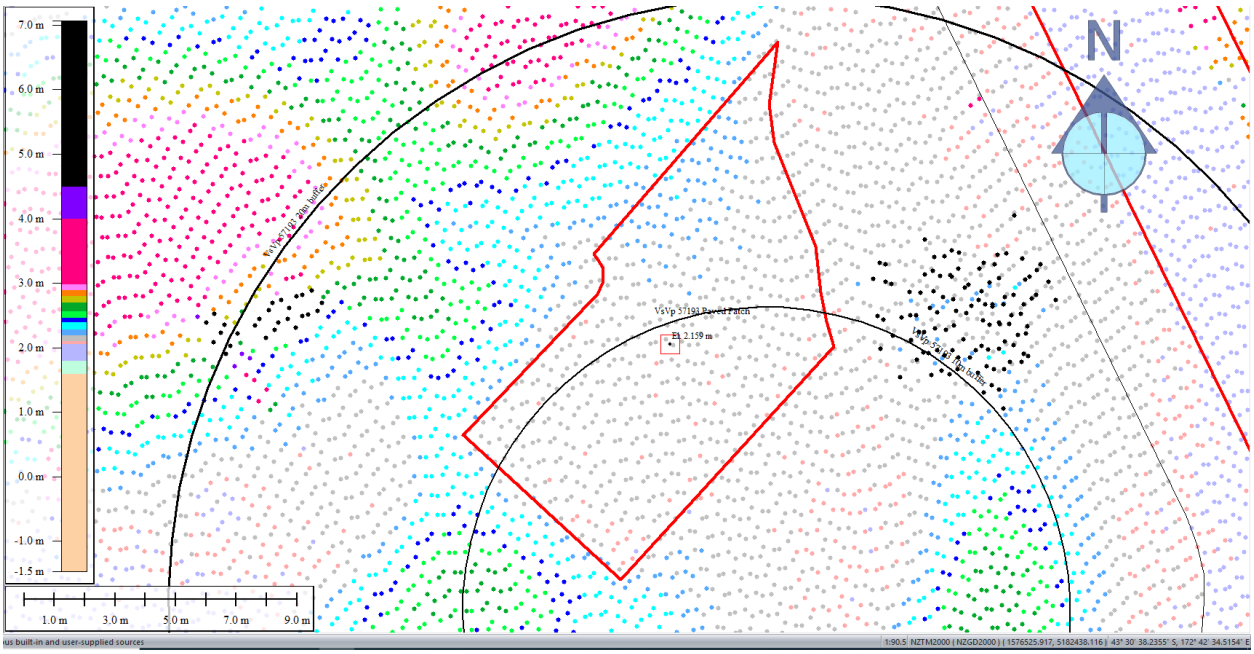

Figure 59: Ground surface elevation averaged over Paved Patch for Oct 2015 LiDAR survey.

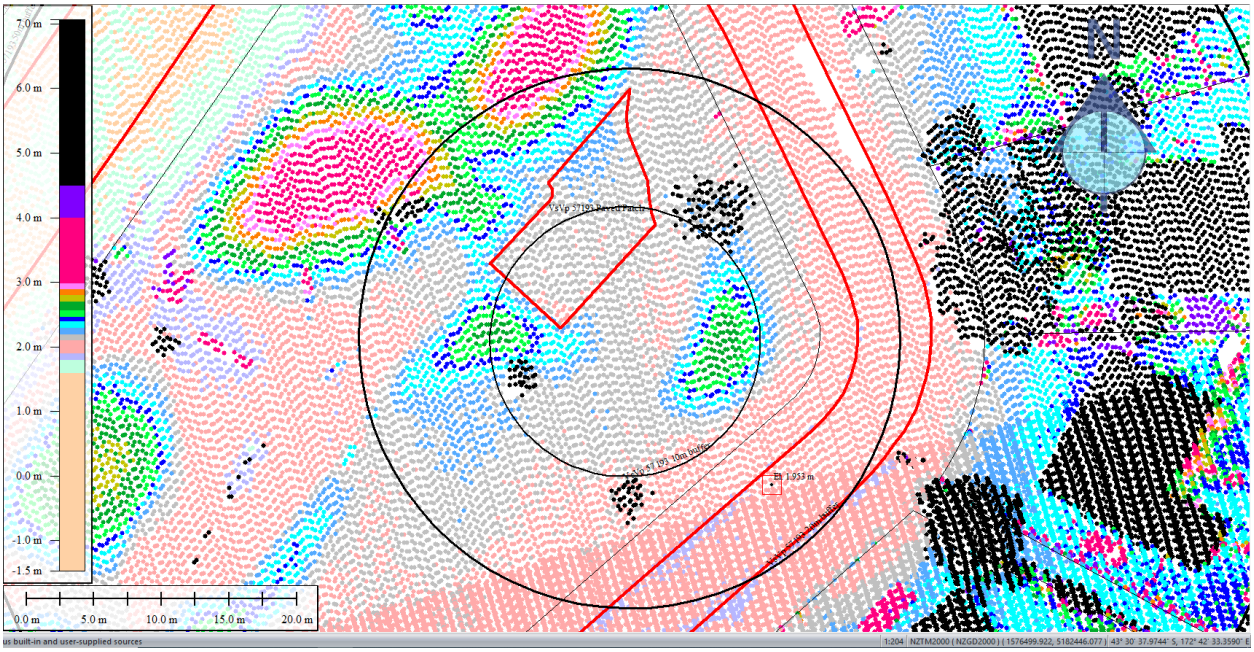

Figure 60: Ground surface elevation averaged over the 20-m buffer for Road for Oct 2015 LiDAR survey.

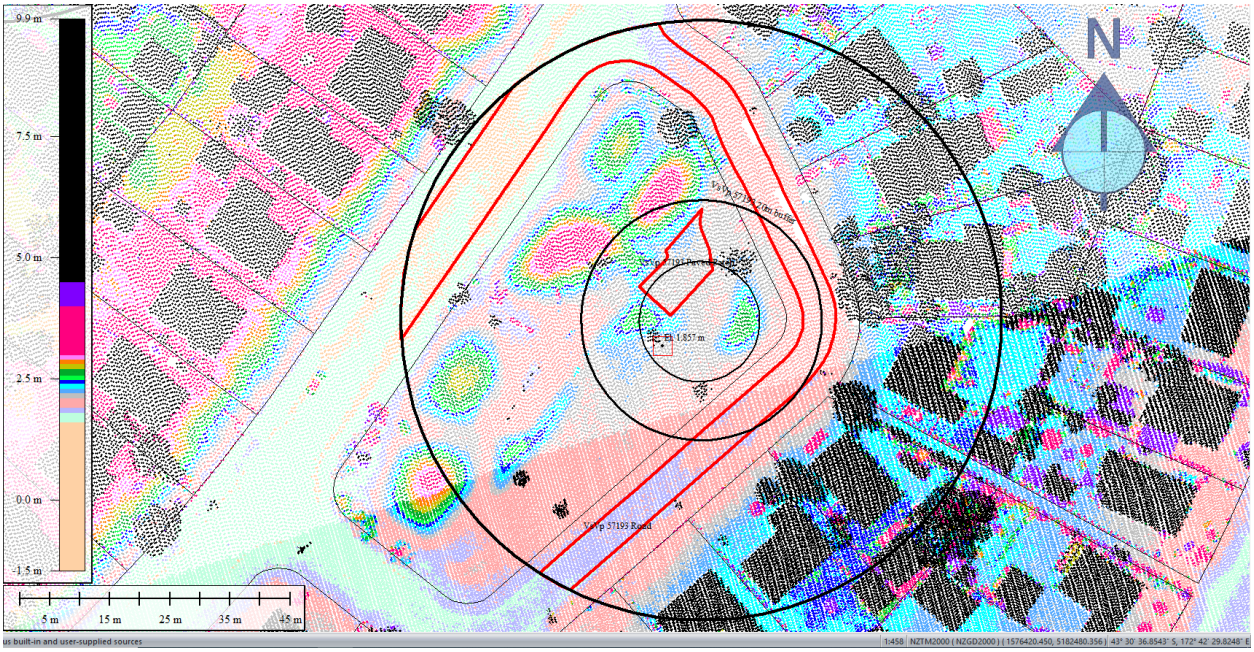

Figure 61: Ground surface elevation averaged over the 50-m buffer for Road for Oct 2015 LiDAR survey.

Figure 62: Satellite image of the site from Oct 2009 showing the basketball court inundated with soil sediments.

Figure 63: Satellite image for Sep-10 EQ (the pooled water on the basketball court is likely from showers of rain on 3 Sep 2010 and the sediments were likely present prior to the Sep-10 EQ as shown in Figure 62).

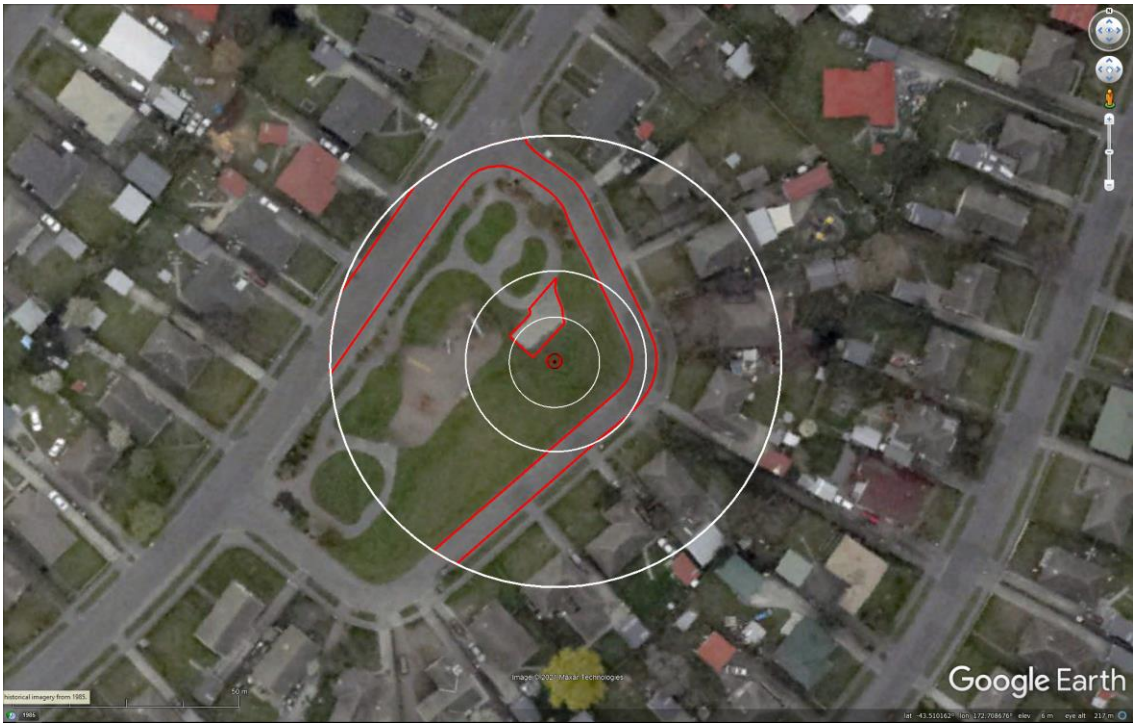

Figure 64: Ejecta outline for Sep-10 EQ.

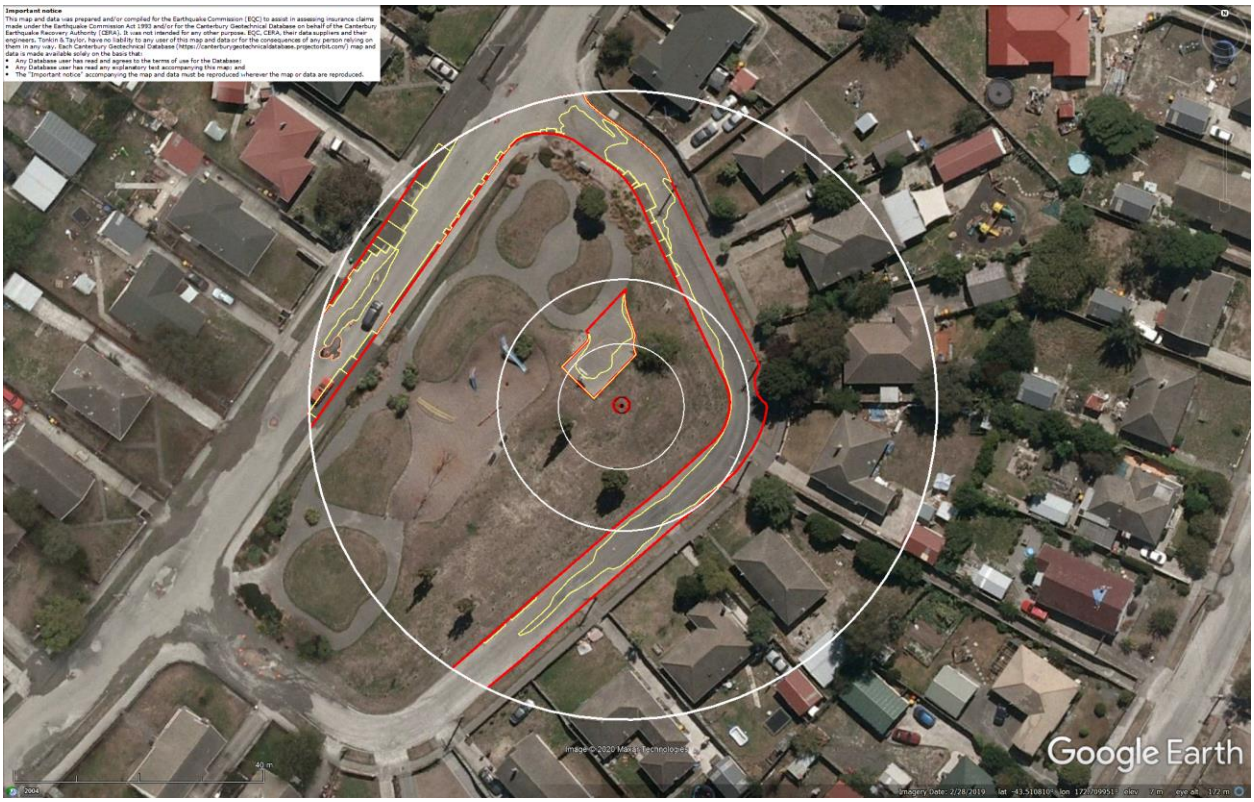

Figure 65: Ejecta outline for Feb-11 EQ.

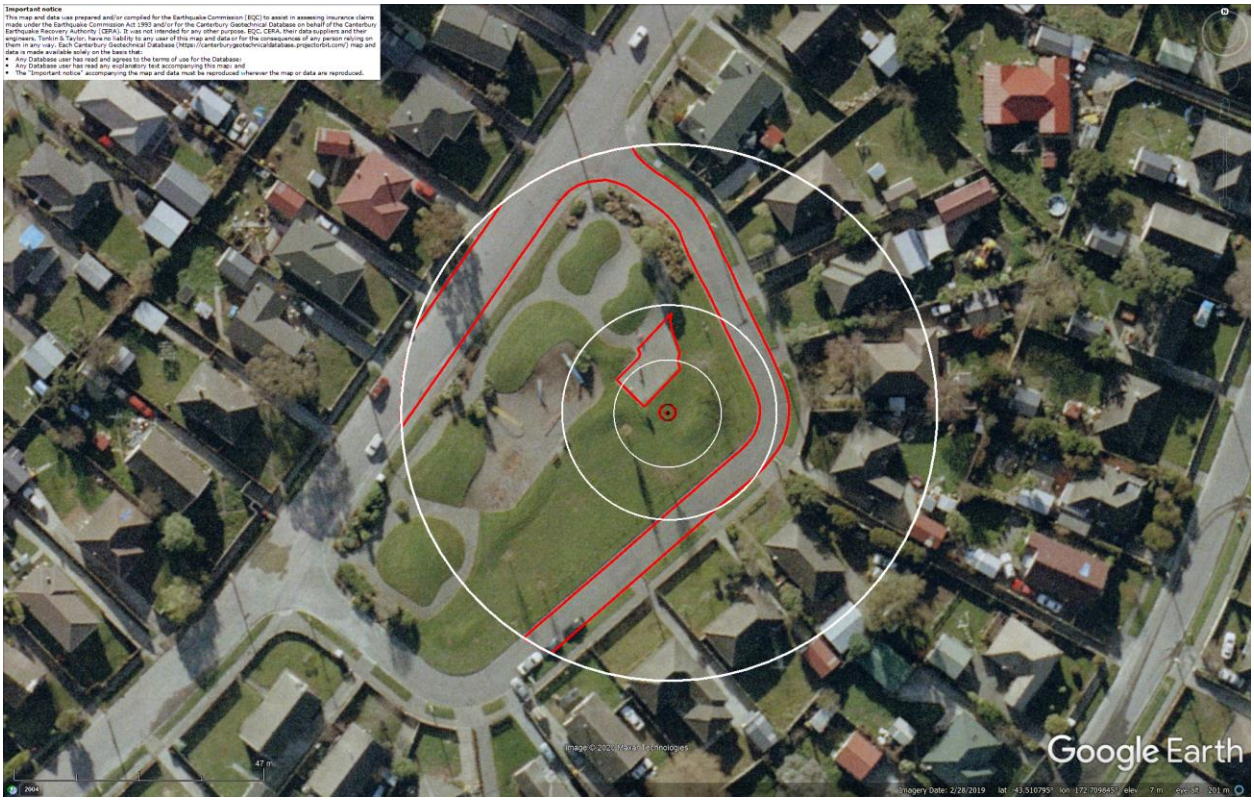

Figure 66: Aerial photograph from 16-06-2011 showing no ejecta at the site for Jun-11 EQ.

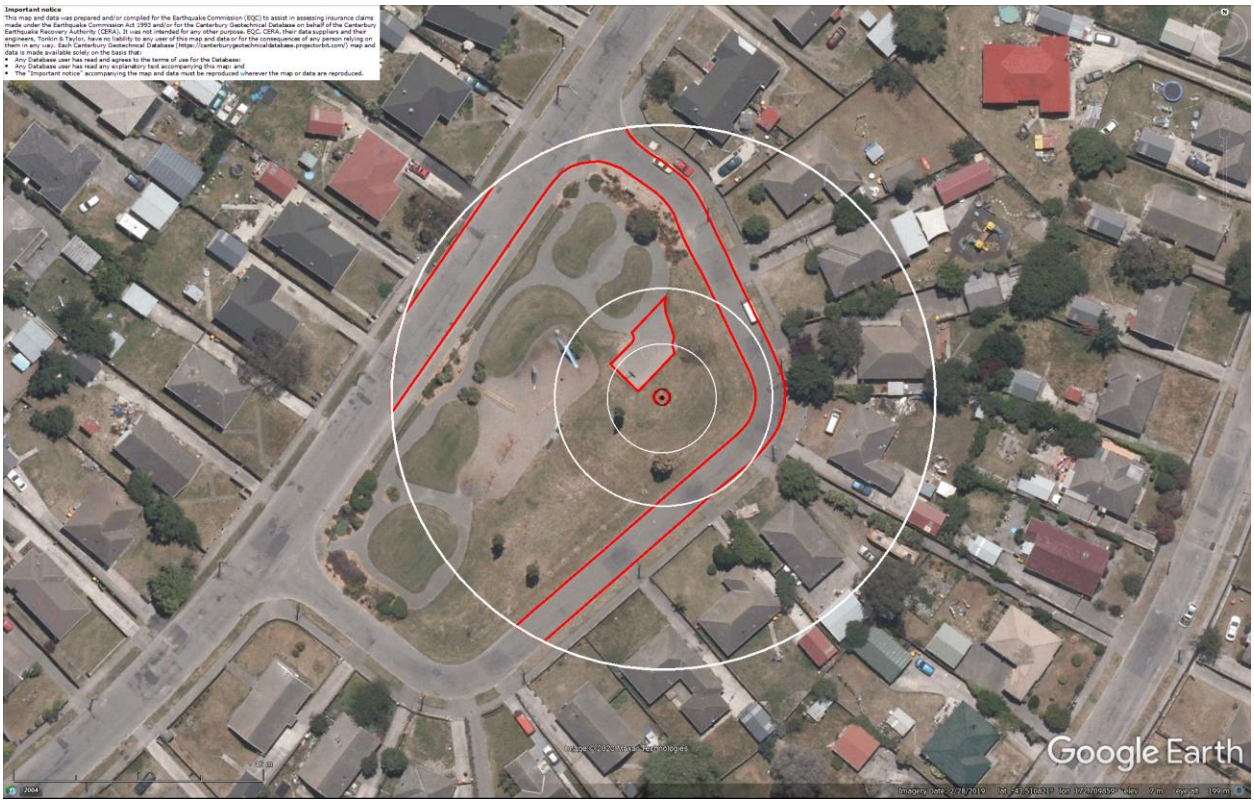

Figure 67: Aerial photograph showing no ejecta for Dec-11 EQ.

Figure 68: View of the basketball court.

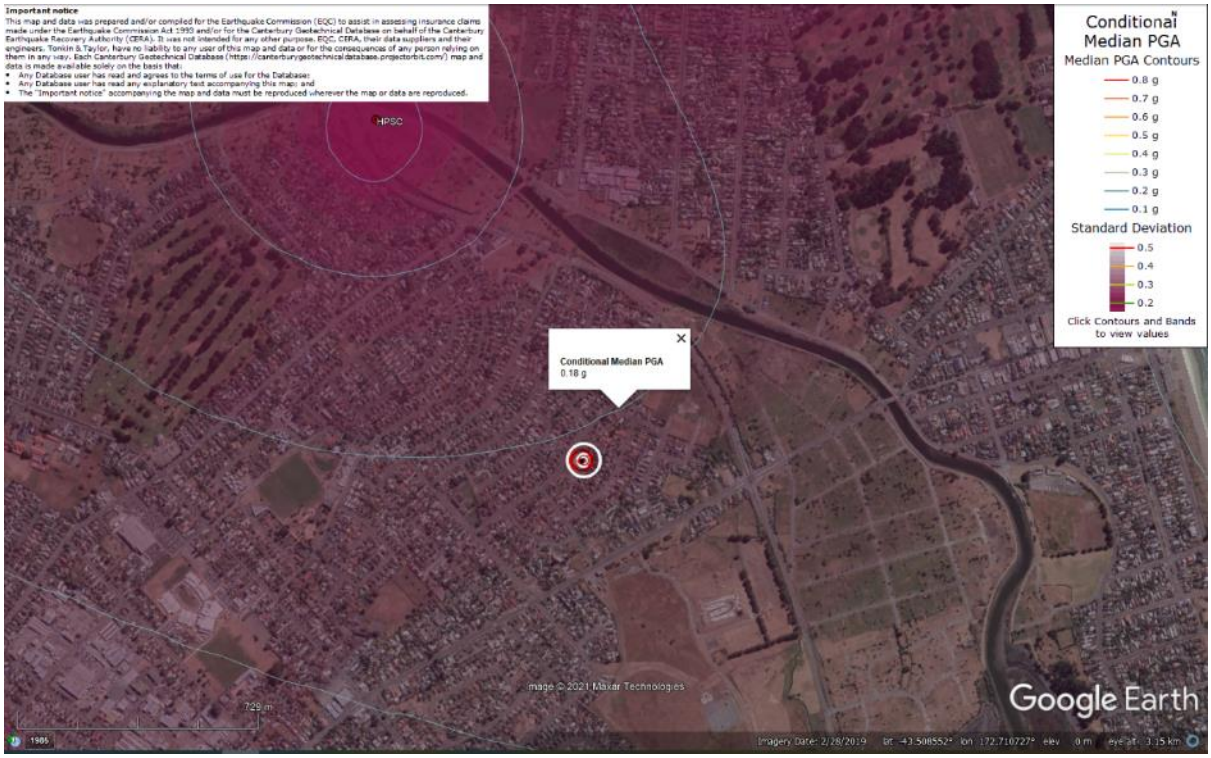

Figure 69: PGA for Sep-10 EQ (st. dev. = 0.300-0.325 ln units).

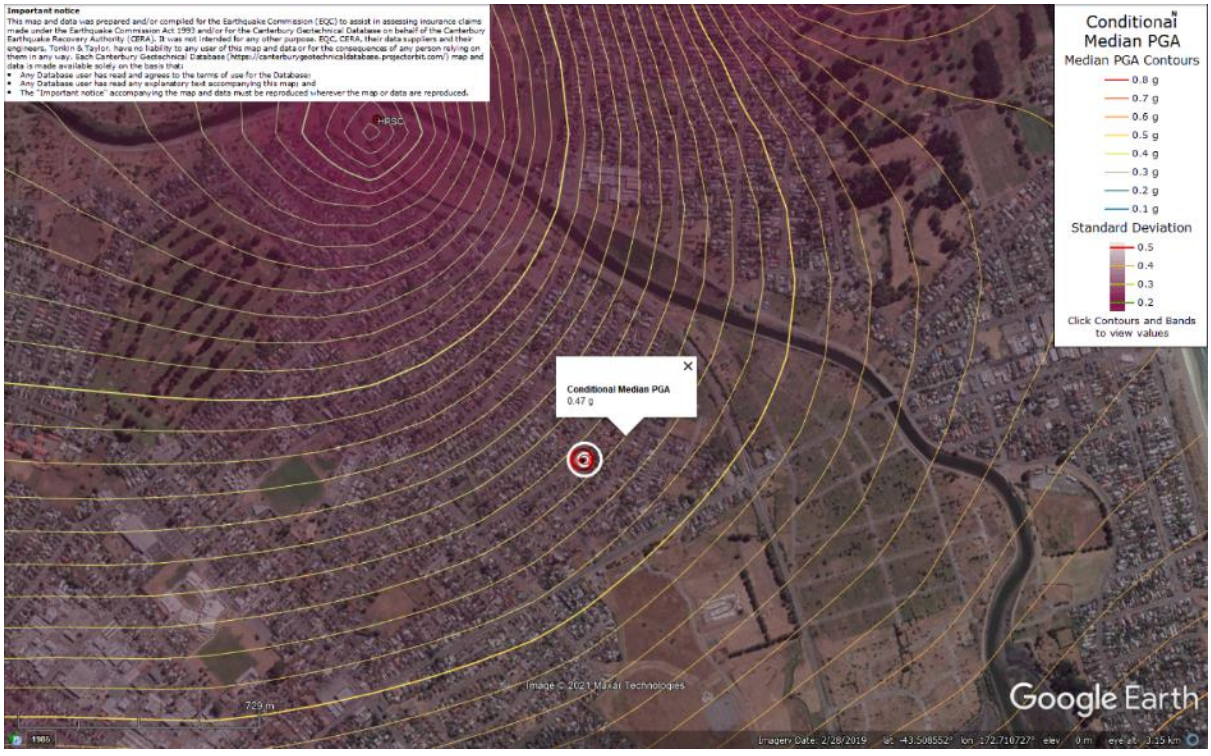

Figure 70: PGA for Feb-11 EQ (st. dev. = 0.325-0.350 ln units).

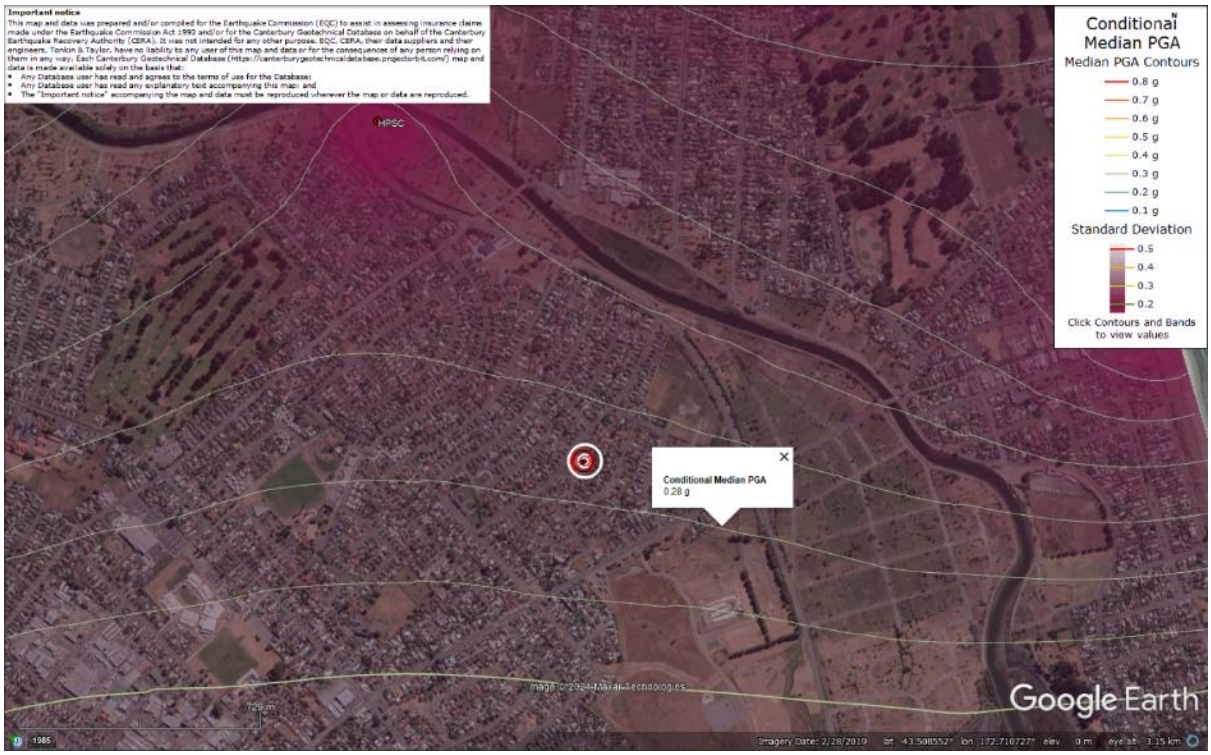

Figure 71: PGA for Jun-11 EQ (st. dev. = 0.325-0.350 ln units).

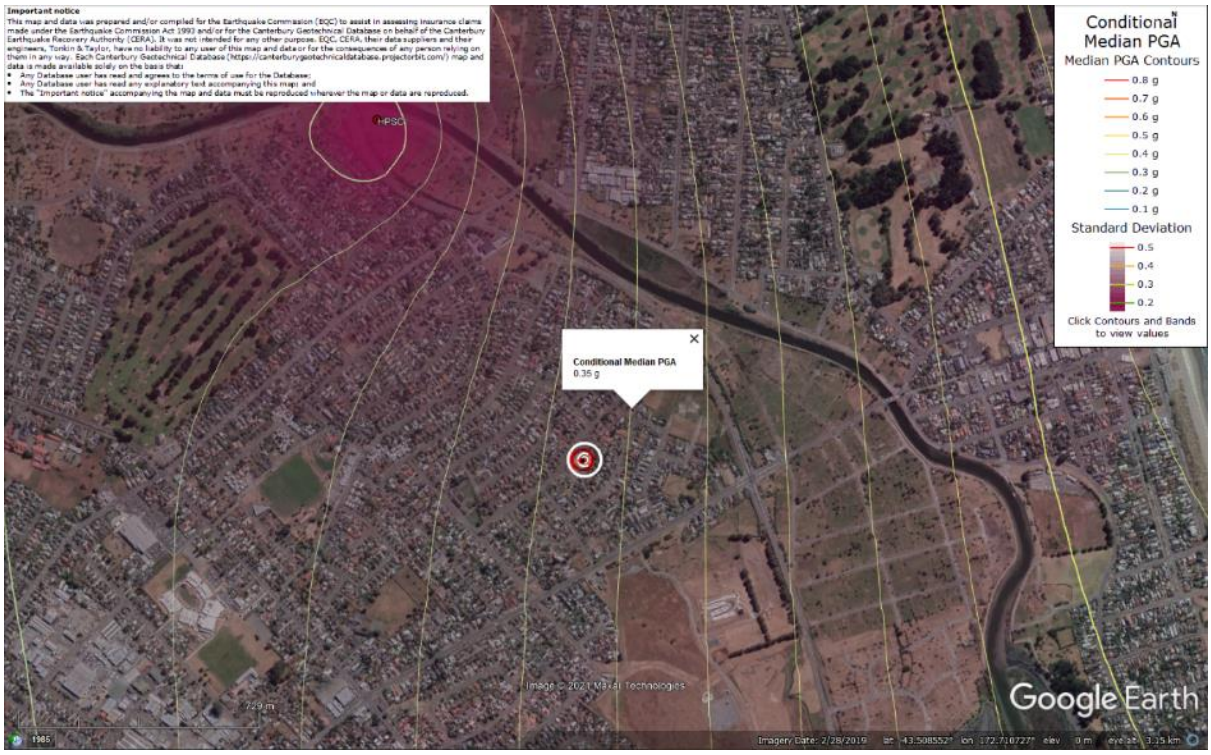

Figure 72: PGA for Dec-11 EQ (st. dev. = 0.350-0.400 ln units).

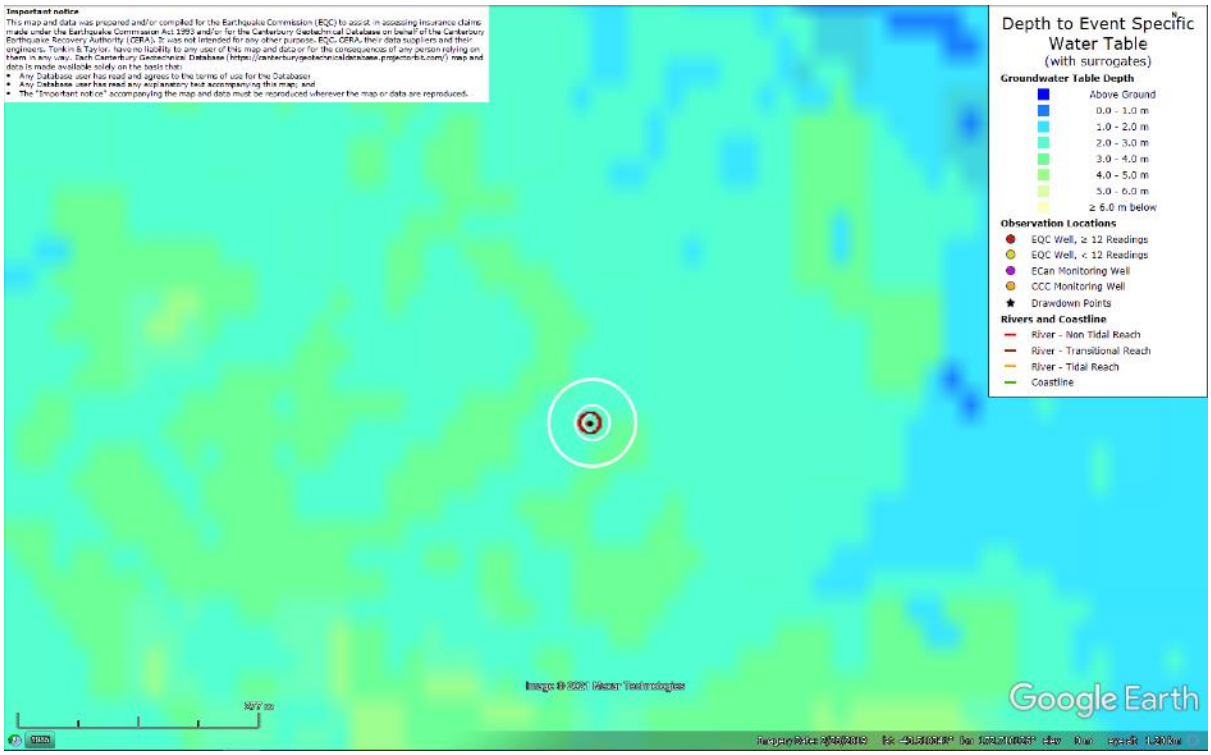

Figure 73: Depth to groundwater table for Sep-10 EQ.

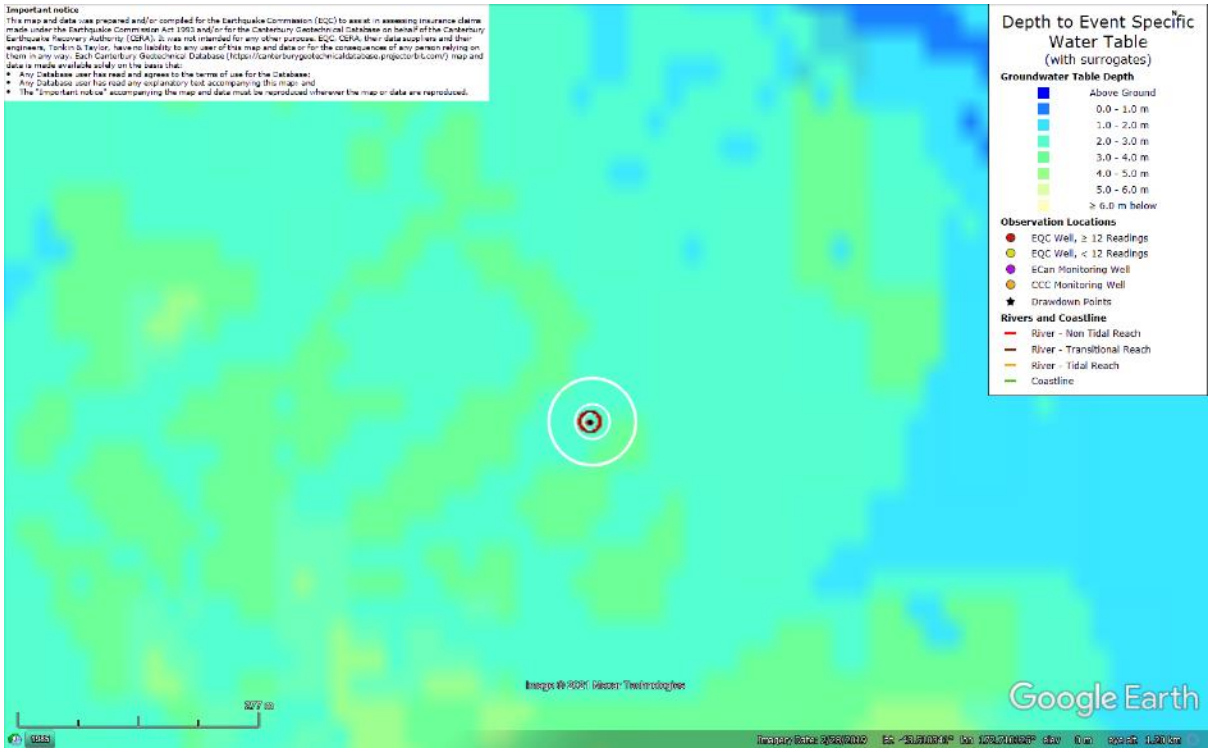

Figure 74: Depth to groundwater table for Feb-11 EQ.

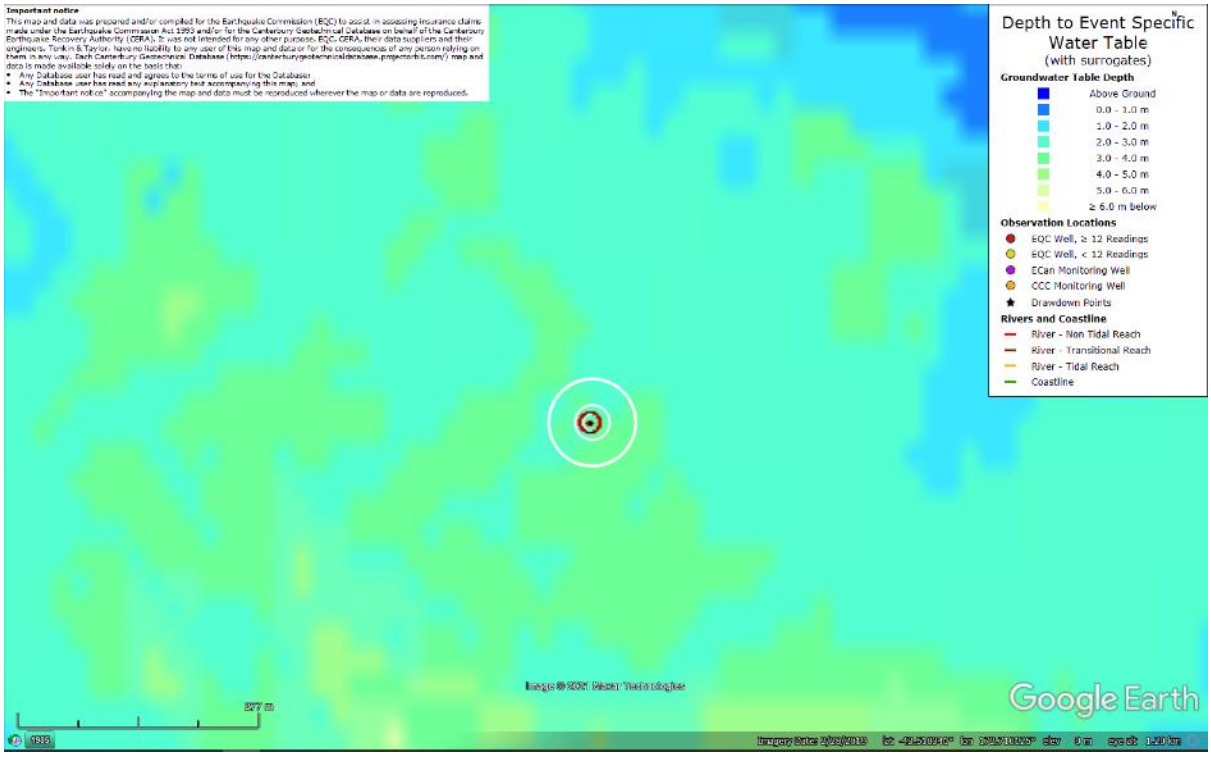

Figure 75: Depth to groundwater table for Jun-11 EQ.

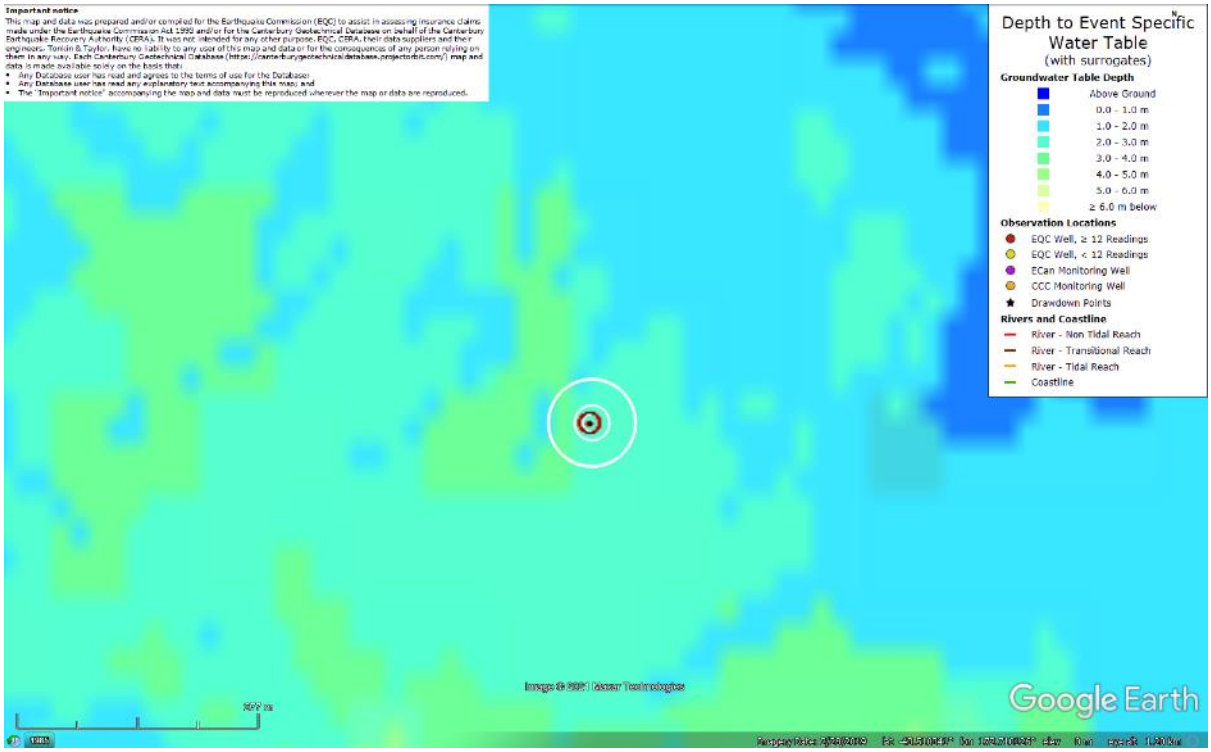

Figure 76: Depth to groundwater table for Dec-11 EQ.

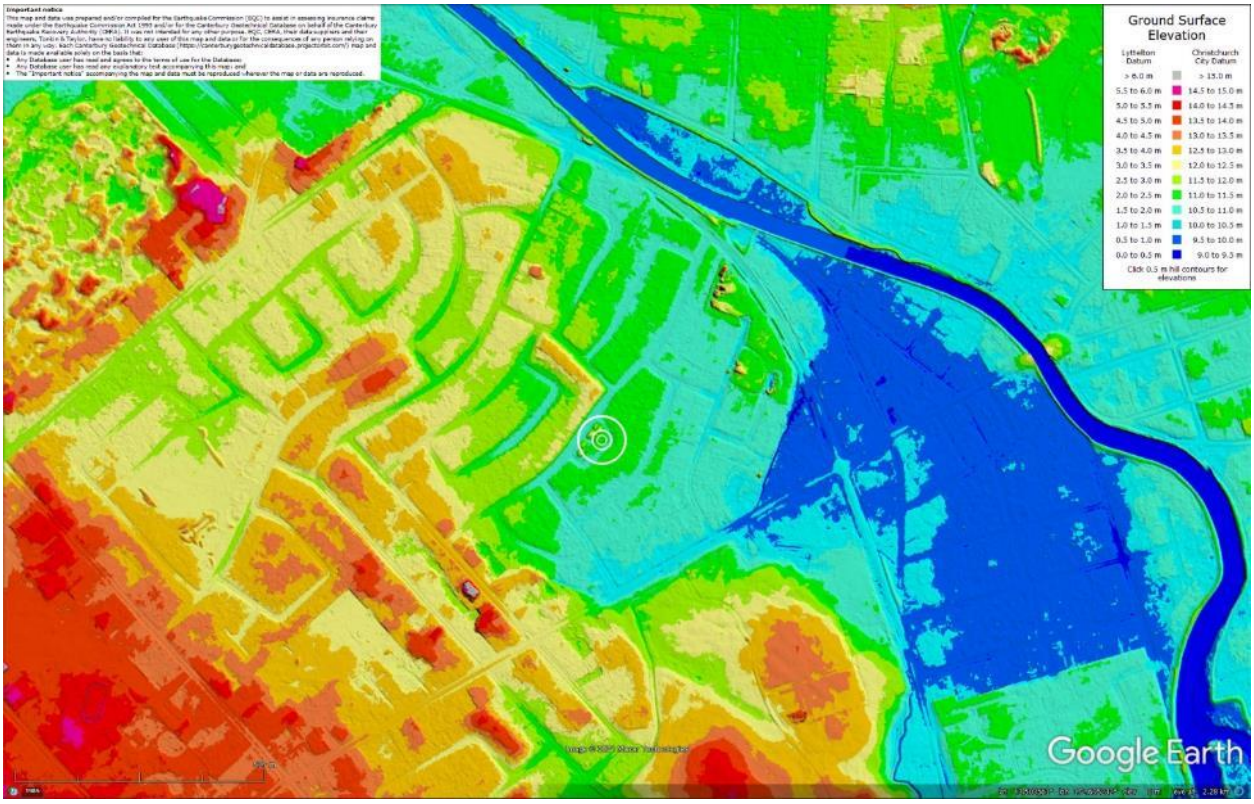

Figure 77: Ground surface elevation according to the Sep-11 LiDAR survey.

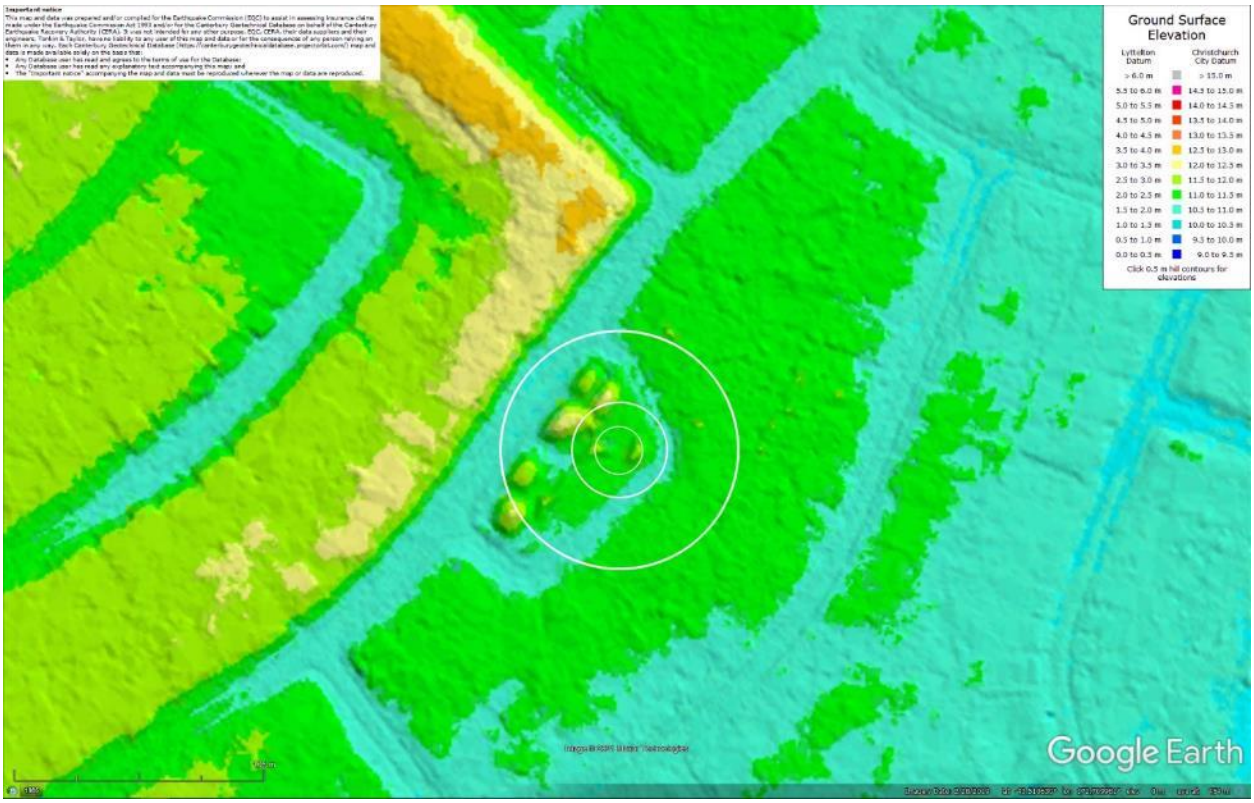

Figure 78: Ground surface elevation according to the Sep-11 LiDAR survey (enlarged).

Figure 79: CPT and borehole locations.

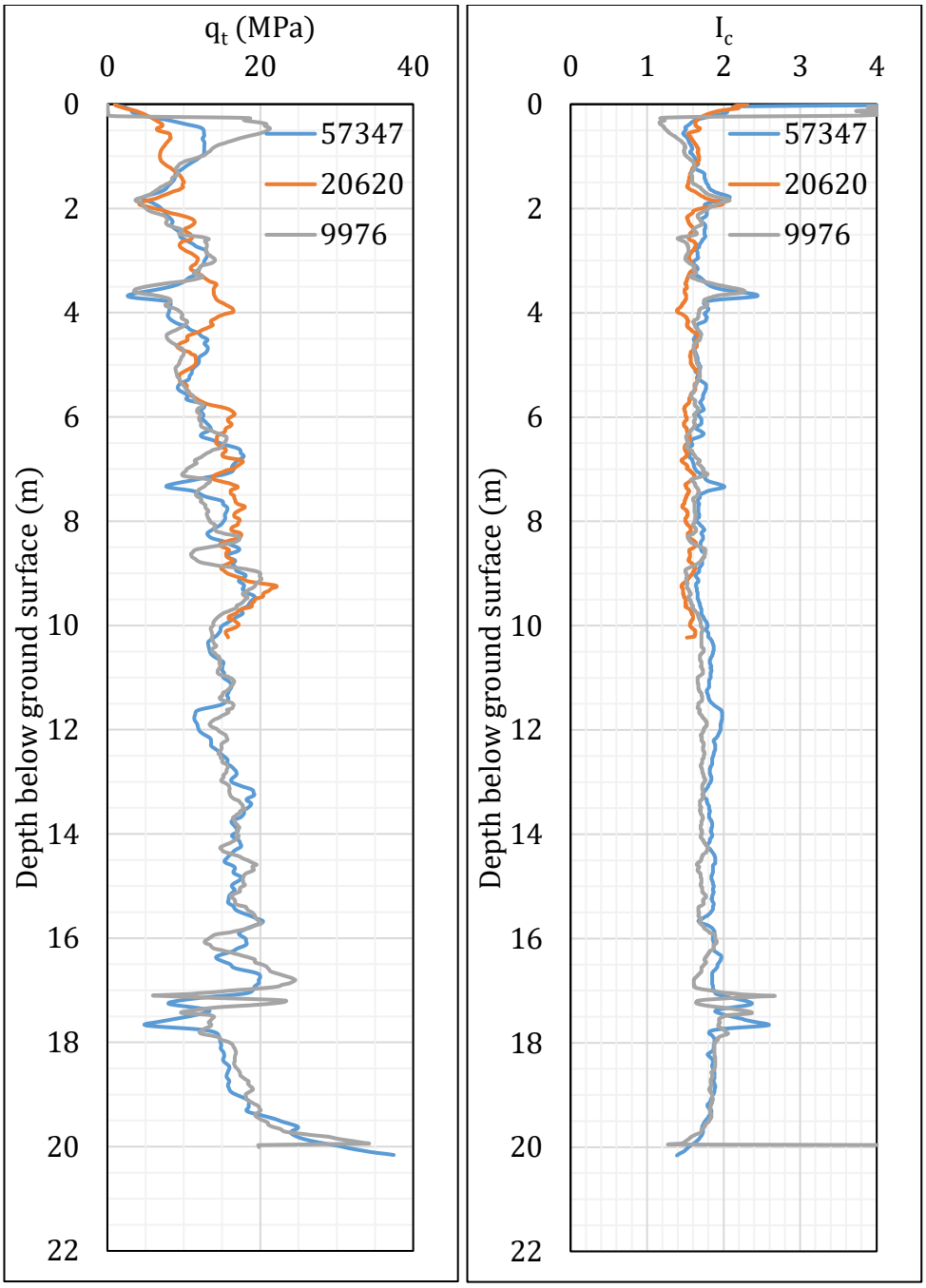

Figure 80: q_t and I_c profiles.

Note 8: The selection of CPTs for the area considered for settlement assessment (Figure 1) is based on the proximity of the CPTs to the considered areas. In accordance with that, the following table shows CPTs that were used for the volumetric settlement analysis in *Cliq v.3.0.3.2*, a CPT soil liquefaction software developed by GeoLogismiki. (The average volumetric settlements were reported in Table 8.)

Table 12: CPT profiles used in volumetric settlement analysis for areas selected for settlement assessment.

CPT ID No.	Concrete Patch	Road
57347 (56587)	✓	✓
20620		✓
9976		✓

Note: CPT 57347 was used to estimate the volumetric settlement between the 10-m and 20-m depth for CPT 20620.

Table 13: CPT-based results.

		CPT ID			
EQ Event	Parameter	57347	20620	9976	$\Delta_{10m-20m}$*
Sep-10	S_{V1D} (mm)	1	0	1	1
	LSN	0	0	0	0
	LPI	0	0	0	0
	LPI_{ish}	0	0	0	--
	$D_{FS<1}$ (m)	undet.	undet.	undet.	--
Feb-11	S_{V1D} (mm)	41	26	105	8
	LSN	7	5	16	1
	LPI	3	2	9	0
	LPI_{ish}	0	2	2	--
	$D_{FS<1}$ (m)	3.58	4.41	3.47	--
Jun-11	S_{V1D} (mm)	3	3	11	2
	LSN	1	1	2	0
	LPI	0	0	0	0
	LPI_{ish}	0	0	0	--
	$D_{FS<1}$ (m)	undet.	undet.	undet.	--
Dec-11	S_{V1D} (mm)	7	1	9	4
	LSN	1	0	2	0
	LPI	0	0	0	0
	LPI_{ish}	0	0	0	--
	$D_{FS<1}$ (m)	undet.	undet.	undet.	--

Notes: $D_{FS<1}$ = Depth to the first liquefiable layer ($FS_L<1$) that is at least 200-mm thick, as determined by the Boulanger and Idriss (2016) liquefaction-triggering procedure (P_L=50%, C_{FC}=0.13, and $I_{c,cutoff}$ =2.6), and exported from *Cliq v.3.0.3.2*; undet. = the specified soil layer was not detected; * indicates the amount of S_{V1D}, LSN, and LPI to be added to CPT 20620 due to its penetration depth being shallower than 20 m.

Note 9: Based on the borehole log (BH 57243, Figure 79), the groundwater table is at a depth of 1.8 m below the ground surface. The ground subsurface profile consists of (1) topsoil (organic silt) to a depth of 0.5 m and (2) fine to medium sand, SP, of the Christchurch formation to a depth of 11.05 m (the end of the borehole). The nearby borehole (BH 4417) suggests that the SP stratum extends to a 20-m depth.

Note 10: The ejecta-induced free-field settlement provided in Table 11 is an areal average settlement due to ejecta, which is based on the total settlement assessment area, A_T (provided in Table 9 and repeated in Table 14). However, the considered area was not always covered completely with ejecta; thus, it is important to provide the localized ejecta-induced settlement, too. The localized settlement due to ejecta is estimated using photographic evidence only as

$$S_{E,P\_localized} = \frac{V_E}{A_E}$$

where V_E is the total volume of ejecta within A_T and A_E is the total coverage area of ejecta within A_T. Please note that the areal ejecta-induced settlement provided in Table 14 as S_{E,P_areal} is the same as $S_{E,P}$ in Table 11, which was estimated as

$$S_{E,P\_areal} = S_{E,P} = \frac{V_E}{A_T}$$

where V_E is the total volume of ejecta within A_T and A_T is the total settlement assessment area.

Table 14a: Areal and localized ejecta-induced settlement estimates for C. Patch (20-m and 50-m buffers) based on photographic evidence.

Earthquake Event	A_T (m^2)	A_E (m^2)	V_E (m^3)	S_{E,P_areal} (mm)	$S_{E,P\_localized}$ (mm)
Sep-10	96.9	0	0	0	0
Feb-11	96.9	37.9	0.1-0.2	<5	5±5
Jun-11	96.9	0	0	0	0
Dec-11	96.9	0	0	0	0

Notes: $S_{E,P\_areal} = S_{E,P}$ reported in Table 11 = areal ejecta-induced settlement; $S_{E,P\_localized}$ = localized ejecta-induced settlement; A_T = total settlement assessment area; V_E = total volume of ejecta within A_T; A_E = total area of ejecta within A_T; The estimates of both areal and localized ejecta-induced settlement are rounded to the nearest 5; Final plus/minus values are also rounded to the nearest 5.

Table 14b: Areal and localized ejecta-induced settlement estimates for Road (20-m buffer) based on photographic evidence.

Earthquake Event	A_T (m^2)	A_E (m^2)	V_E (m^3)	S_{E,P_areal} (mm)	$S_{E,P\_localized}$ (mm)
Sep-10	182	0	0	0	0
Feb-11	187	49.4	0.2-0.3	<5	5±5
Jun-11	182	0	0	0	0
Dec-11	182	0	0	0	0

Notes: S_{E,P_areal} = $S_{E,P}$ reported in Table 11 = areal ejecta-induced settlement; $S_{E,P\_localized}$ = localized ejecta-induced settlement; A_T = total settlement assessment area; V_E = total volume of ejecta within A_T; A_E = total area of ejecta within A_T; The estimates of both areal and localized ejecta-induced settlement are rounded to the nearest 5; Final plus/minus values are also rounded to the nearest 5.

Table 14c: Areal and localized ejecta-induced settlement estimates for Road (50-m buffer) based on photographic evidence.

Earthquake Event	A_T (m^2)	A_E (m^2)	V_E (m^3)	S_{E,P_areal} (mm)	$S_{E,P\_localized}$ (mm)
Sep-10	1096	0	0	0	0
Feb-11	1191	777	5.9-10.1	5±5	10±5
Jun-11	1096	0	0	0	0
Dec-11	1096	0	0	0	0

Notes: S_{E,P_areal} = $S_{E,P}$ reported in Table 11 = areal ejecta-induced settlement; $S_{E,P\_localized}$ = localized ejecta-induced settlement; A_T = total settlement assessment area; V_E = total volume of ejecta within A_T; A_E = total area of ejecta within A_T; The estimates of both areal and localized ejecta-induced settlement are rounded to the nearest 5; Final plus/minus values are also rounded to the nearest 5.

Summary 2:

The best estimate of the localized ejecta-induced free-field ground settlement at the Carisbrooke Playground St site for the SEP 2010, FEB 2011, JUN 2011, and DEC 2011 earthquake is 0 mm, 5±5 mm, 0 mm, and 0 mm, respectively.